SANDIA REPORT

SAND2009-1986
Unlimited Release
Printed April 2009

Analysis of Cavern Stability at the Bryan Mound SPR Site

Steven R. Sobolik and Brian L. Ehgartner

Prepared by
Sandia National Laboratories
Albuquerque, New Mexico 87185 and Livermore, California 94550

Sandia is a multiprogram laboratory operated by Sandia Corporation,
a Lockheed Martin Company, for the United States Department of Energy's
National Nuclear Security Administration under Contract DE-AC04-94AL85000.

Issued by Sandia National Laboratories, operated for the United States Department of Energy by Sandia Corporation.

Available to DOE and DOE contractors from
U.S. Department of Energy
Office of Scientific and Technical Information
P.O. Box 62
Oak Ridge, TN 37831

Telephone: (865) 576-8401
Facsimile: (865) 576-5728
E-Mail: reports@adonis.osti.gov
Online ordering: http://www.osti.gov/bridge

Available to the public from
U.S. Department of Commerce
National Technical Information Service
5285 Port Royal Rd.
Springfield, VA 22161

Telephone: (800) 553-6847
Facsimile: (703) 605-6900
E-Mail: orders@ntis.fedworld.gov
Online order: http://www.ntis.gov/help/ordermethods.asp?loc=7-4-0#online

SAND2009-1986
Unlimited Release
Printed April 2009

Analysis of Cavern Stability at the Bryan Mound SPR Site

Steven R. Sobolik and Brian L. Ehgartner
Energy, Resources, and Systems Analysis Center
Sandia National Laboratories
P.O. Box 5800
Albuquerque, New Mexico 87185-0751

ABSTRACT

This report presents computational analyses that simulate the structural response of caverns at the Strategic Petroleum Reserve Bryan Mound site. The cavern field comprises 20 caverns. Five caverns (1, 2, 4, and 5; 3 was later plugged and abandoned) were acquired from industry and have unusual shapes and a history dating back to 1946. The other 16 caverns (101-116) were leached according to SPR standards in the mid-1980s and have tall cylindrical shapes. The history of the caverns and their shapes are simulated in a 3-D geomechanics model of the site that predicts deformations, strains, and stresses. Future leaching scenarios due to oil drawdowns using fresh water are also simulated by increasing the volume of the caverns. Cavern pressures are varied in the model to capture operational practices in the field. The results of the finite element model are interpreted to provide information on the current and future status of subsidence, well integrity, and cavern stability.

The most significant result in this report is relevant to caverns 1, 2, and 5. The caverns have non-cylindrical shapes and have potential regions where the surrounding salt may be damaged during workover procedures. During a workover the normal cavern operating pressure is lowered to service a well. At this point the wellhead pressures are atmospheric. When the workover is complete, the cavern is repressurized. The resulting elastic stresses are sufficient to cause tension and large deviatoric stresses at several locations. With time, these stresses relax to a compressive state due to salt creep. However, the potential for salt damage and fracturing exists. The analyses predict tensile stresses at locations with sharp-edges in the wall geometry, or in the case of cavern 5, in the neck region between the upper and lower lobes of the cavern. The effects do not appear to be large-scale, however, so the only major impact is the potential for stress-induced salt falls in cavern 5, potentially leading to hanging string damage. Caverns 1 and 2 have no significant issues regarding leachings due to drawdowns; cavern 5 may require a targeted leaching of the neck region to improve cavern stability and lessen hanging string failure potential. The remaining caverns have no significant issues regarding cavern stability and may be safely enlarged during subsequent oil drawdowns. Well strains are significant and consequently future remedial actions may be necessary. Well strains certainly suggest the need for appropriate monitoring through a well-logging program. Subsidence is currently being monitored; there are no issues identified regarding damage from surface subsidence or horizontal strain to surface facilities.

ACKNOWLEDGEMENTS

The authors would like to thank Darrell Munson and David Borns for their review and support of this work.

TABLE OF CONTENTS

LIST OF FIGURES

LIST OF TABLES

1. INTRODUCTION

1.1 OBJECTIVE

The U.S. Department of Energy (DOE) Strategic Petroleum Reserve (SPR) stores crude oil in solution-mined caverns in the salt dome formations of the Gulf Coast. There are a total of 62 caverns located at four different sites in Texas (Bryan Mound and Big Hill) and Louisiana (Bayou Choctaw and West Hackberry), as shown in Figure 1. Each cavern is constructed and then operated using casings inserted through a well bore or well bores that are lined from the surface to near the top of the cavern with steel casings cemented in place. The Bryan Mound salt dome, located approximately 60 miles south of Houston, Texas, near the city of Freeport, is the largest of the SPR sites in terms of oil-storage capacity (currently 226 million barrels). Sandia National Laboratories (SNL), as the geotechnical advisor to the DOE SPR Project Office, conducts site-characterization investigations and other longer-term geotechnical and engineering studies in support of the program.

The SPR sites, as well as most other oil and natural gas storage sites in salt domes along the Gulf Coast, are varied in terms of cavern structure and layout. The Bryan Mound SPR site was acquired by DOE, by condemnation, in April 1977 from the Freeport Mineral Company and other owners. At that time there were five caverns at the site. An analysis of these existing Phase 1 caverns from 1977 to 1979 resulted in four of them being certified for crude oil storage. As early as October 1977 oil injection commenced at the site. After purchase of the site, additional caverns were leached using standards that resulted in tall cylindrical shaped caverns; these caverns, numbered 101 through 116, are referred to in this report as Phase 2 or post-1981 caverns. This report describes three-dimensional (3-D) geomechanical calculations modeling the long-term behavior of the Bryan Mound SPR site in response to changing oil pressure conditions in the storage caverns and future growth of the caverns through subsequent leaching. This analysis evaluates the stress and deformation history of the caverns to the present day, and predicts the effects on cavern stability and well strain of subsequently enlarging the caverns.

When the SPR took ownership of the Phase 1 caverns in 1981, finite element analyses were performed to assess the long-term performance and stability of the caverns (Preece and Foley, 1984). The analyses were two-dimensional axisymmetric idealizations and each cavern was simulated independently of the others. The failure function was based on an accumulated strain as a function of pressure. While the analyses at that time predicted stability, cavern workover conditions were not simulated. Today's capabilities extend far beyond those original analyses. The current analyses simulate the entire cavern field with realistic cavern shapes in 3-D and thus capture cavern interactions. The model presented herein also includes the drop in cavern pressures during workovers, an obvious adverse condition for the caverns from a closure and stability point of view. In addition, the rock mechanics community has migrated away from accumulated strain based failure criteria for salt in favor of a stress criterion, and a large data base now exists to support the merits of that criterion. The technology has dramatically improved since the 1980's and since that time, SPR has collected cavern and subsidence data that enable comparison of model predictions to actual cavern and surface deformations. This

information enables a calibration of the model to field data and results in a much more accurate assessment of the stress state. The necessity to update the analyses of Bryan Mound is undeniable. The following analyses will provide the best prediction to date of the current and future state of the SPR caverns at Bryan Mound.

Figure 1. Location of SPR sites.

The analysis of the Bryan Mound site differs significantly from previous analyses. The computational domain for this analysis includes all the Bryan Mound caverns and the entire salt dome, as opposed to the previous two-dimensional calculations, or three-dimensional calculations that used a 30-degree wedge to simulate a symmetric 19-cavern field geometry of West Hackberry (Ehgartner and Sobolik, 2002). All of the caverns in this analysis are meshed with geometries based on sonar data measurements. The entire lives of the caverns (construction, brine or oil storage, operating and workover pressures) are modeled individually for each cavern. Finally, the sandstone that surrounds the salt dome is included in this analysis, providing a realistic far-field stress boundary condition.

For these analyses, each of the caverns (except 5) experiences five leaching operations to develop the cavern, with a volume growth of approximately 15% for each leach (there are departures from this scenario for a few caverns; these departures are detailed later in the report). The leaching operations are simulated to begin in September 2008.

Four measures of cavern performance are evaluated in this study. The first measure uses dilatant damage factors as identified by a damage criterion, a linear function of the hydrostatic pressure (Van Sambeek et al., 1993). The second performance measure looks at cavern volume closure for each cavern. The third measure evaluates the axial well strain in the caprock above the cavern, and the fourth measure looks at the maximum subsidence at the surface for each cavern. The long-term stability of the Bryan Mound caverns, particularly for possible cavern volume expansion by leaching during oil drawdowns, will be evaluated using these criteria.

1.2 REPORT ORGANIZATION

This report is organized in the following fashion: Section 2 gives a brief description of the Bryan Mound cavern site to show the diversity of cavern geometries. Section 3 describes the analytical model, including the cavern designs, stratigraphy, material models, material properties, and damage criteria used for the analyses. Section 4 shows the results of the calculations, and identifies failure modes for the salt and the casings. Section 5 summarizes the results, and provides concluding remarks.

2. SITE DESCRIPTION

The Bryan Mound salt dome, located approximately 60 miles south of Houston, Texas, near the city of Freeport, is the largest of the SPR sites in terms of oil-storage capacity (currently 226 million barrels). The geological characteristics related to the Bryan Mound site were first described by Hogan (1980). Neal et al. (1994) utilized the earlier work, together with additional information on dome geology, surrounding stratigraphy, and relevant environmental information, to update the dome characterization. Conversion of the two-dimensional databases from these earlier characterization reports formed the basis for the most recent reexamination by Stein and Rautman (2005) using modern three-dimensional methods for representation of the dome and its surroundings. While major aspects of the dome, caprock and surrounding strata defined by the earlier characterizations remain unchanged, the updated three-dimensional models of Stein and Rautman (2005) used more refined analysis of the data and produced models of the dome that differed slightly from the earlier models. The three-dimensional models also achieve a level of visualization clarity and graphical manipulation previously impossible. Finally, the Bryan Mound caverns have been extensively characterized and mapped in a sonar atlas prepared by Rautman and Lord (2007).

Figure 2 shows a plan view of the Bryan Mound site (Stein and Rautman, 2005) with the cavern's approximate location within the salt dome, and the interface of the salt dome with the caprock and surrounding sandstone. The approximate cavern locations are shown in the plan view. An updated geologic perspective of the salt dome and caprock are provided in Figure 3 (Rautman and Lord, 2007). Note that there seem to be two regions within the salt dome that are possibly separated by a salt spine or shear zone. The thickest caprock regions correspond to the two separate regions inferred from the structure contour map. Further study of the sonar data used to characterize the salt dome reveal the orientation of potential boundary shear zones within the salt dome; these zones are shown in Figure 4 (Rautman and Lord, 2007). Of the three boundary shear zones shown in Figure 4, the one of greatest interest is that which is in the southeast portion of the salt dome, running roughly southwest to northeast. Caverns 106, 109, 112, 113, and 114 are located to the south of this shear zone. This region of the salt dome appears to contain salt with creep properties leading to higher creep rates than the remainder of the dome; the reasons for this difference will be examined in greater detail later in this report.

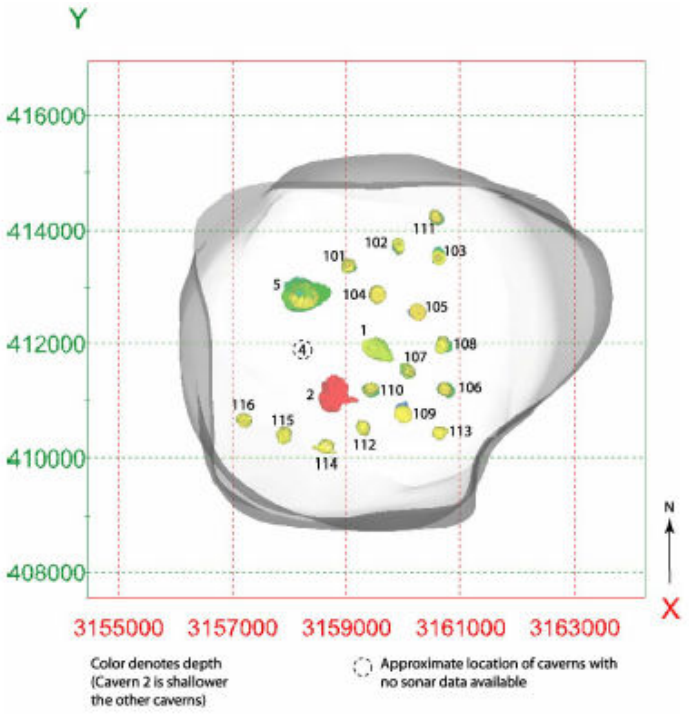

Figure 2. Top view of the Bryan Mound salt dome and selected cavern models. Note that Cavern BM-4 is not represented with a sonar model. (Stein and Rautman, 2005)

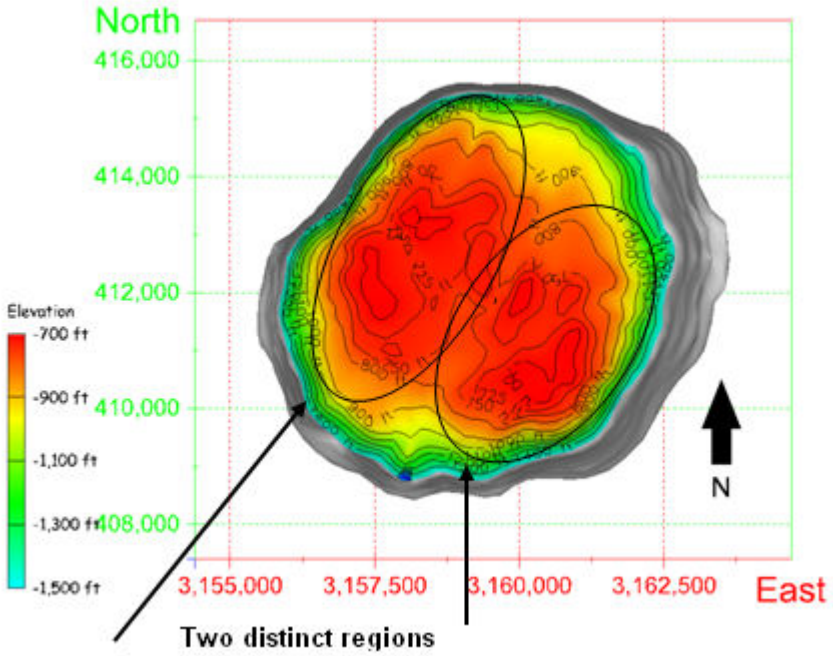

Figure 3. 3-D model of the top of caprock and the top of salt (considered to be bottom of caprock); contours are of caprock thickness in feet (Rautman and Lord, 2007).

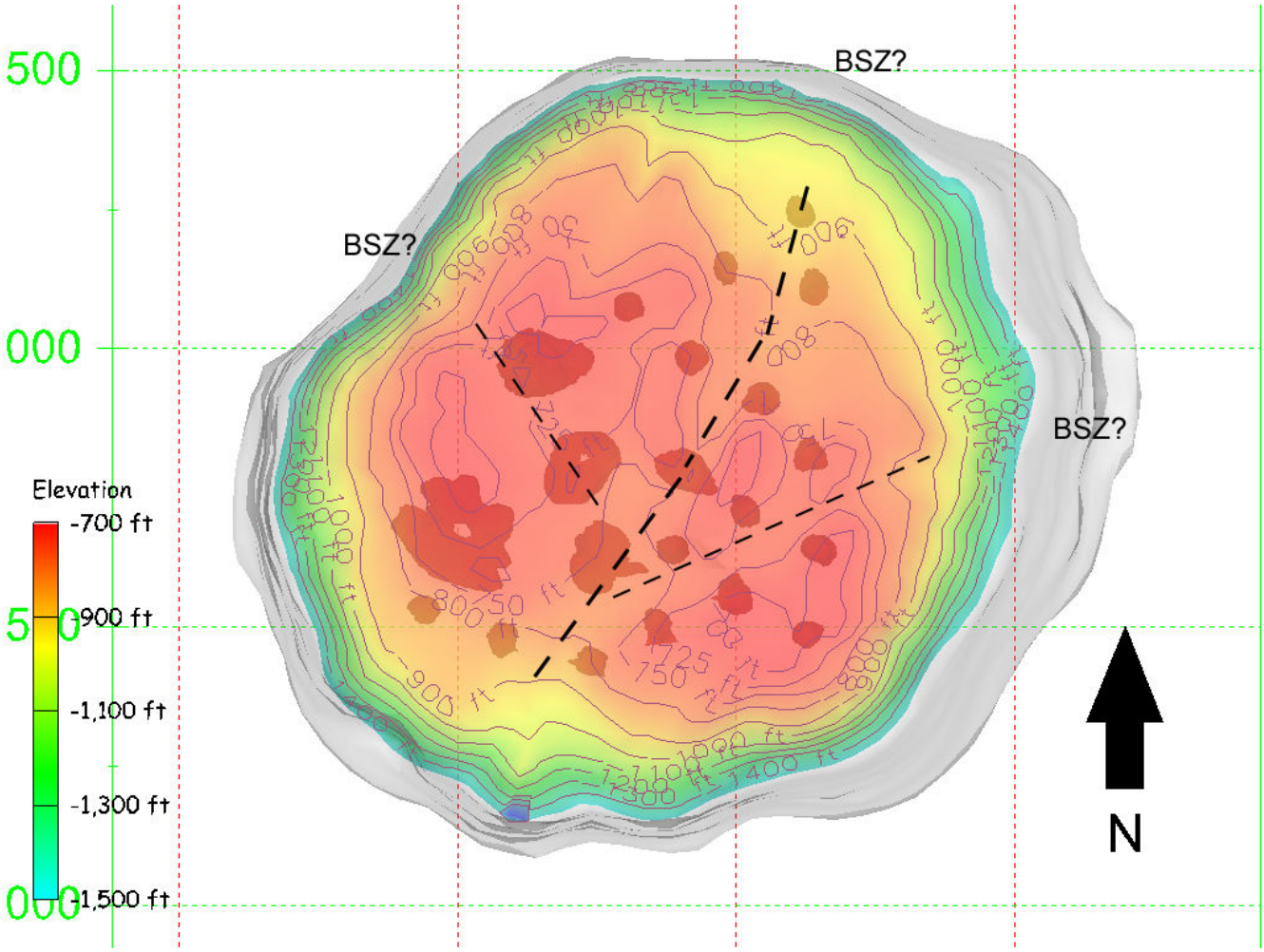

Figure 4. Potential boundary shear zones in the Bryan Mound salt dome (Rautman and Lord, 2007).

Figure 5 shows the cavern layout at the Bryan Mound site (Rautman and Lord, 2007), using the DOE coordinates provided; cavern 4 is located in the cluster of cavern wells between caverns 1, 2, 3, and 5. Figure 6 shows cavern geometries based on sonar measurements obtained through 2007 (Rautman and Lord, 2007). Note the enlarged tops and asymmetries of the cavern shapes. In general, caverns in the SPR are intentionally shaped with larger tops to accommodate future oil drawdowns where only the bottom portions of the caverns are preferentially leached, and hence the overall cavern shape becomes more cylindrical, due to raw water injections to remove the oil. Salt properties also result in unpredictable cavern shapes as the insoluble content or dissolution rates of salt can spatially vary. This explains some of the asymmetries found in the cavern shapes. The Phase 1 caverns were acquired through purchase; these caverns have unusual shapes as they were not intentionally leached for product storage, but were used to produce brine. Clearly a variety of shapes are currently found in the SPR and this variety of cavern shapes will continue through future drawdowns.

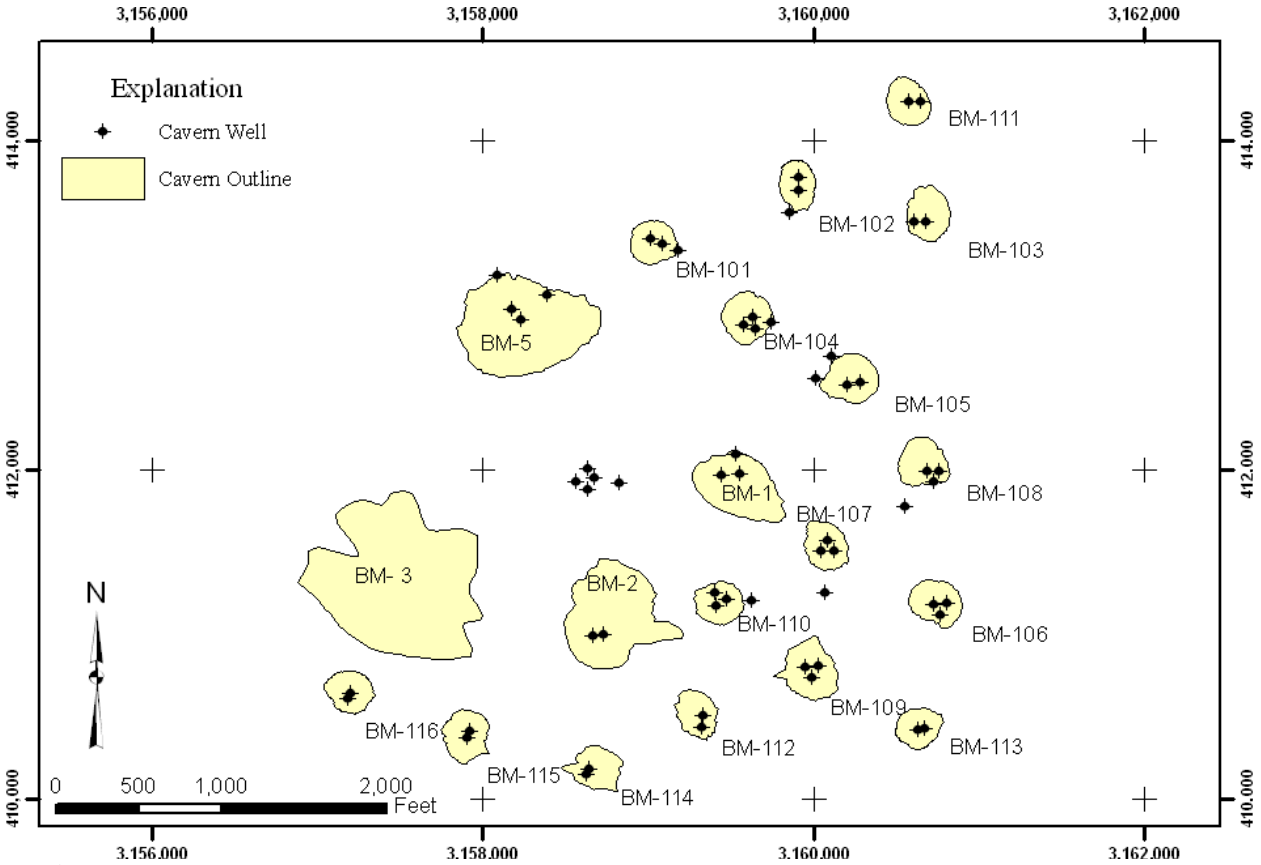

Figure 5. Schematic of the Location of the SPR Caverns at Bryan Mound (Rautman and Lord, 2007)

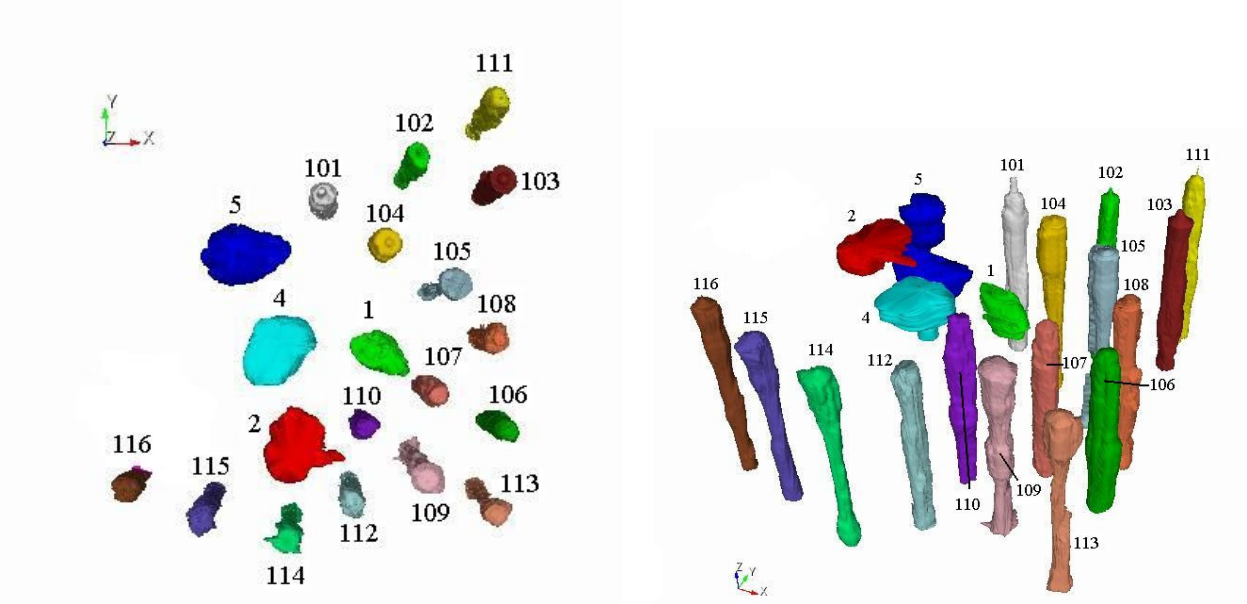

Figure 6. Visualization of the 20 oil-storage caverns at Bryan Mound SPR site.

3. ANALYSIS MODEL

3.1 MODEL DESCRIPTION

In several previous analyses, SPR sites have been modeled using a 30-degree wedge section cut out of a 19-cavern field (Ehgartner and Sobolik, 2002). Such a mesh has been used to apply three-dimensional geometric and geomechanical effects to an SPR cavern field with a minimum of mesh elements (usually under 100,000 elements). Several recent advances now permit a more comprehensive analysis of a salt dome cavern field. First, the computational code JAS3D has been parallelized, allowing for the use of up to 64 CPU nodes for calculations. Second, recent advances in cavern and salt dome geometric visualization based on sonar data allow a realistic representation of cavern geometry. Third, recent advances in meshing capabilities such as mesh cutting allow for converting cavern visualization geometries easily into computational meshes. Because of these advances, a new computational domain has been developed for the Bryan Mound cavern field which encompasses the entire salt dome, including all twenty oil storage caverns.

At the Bryan Mound site, the five caverns known as Phase 1 – caverns 1 through 5 – were created as early as 1946 and were used for brining and storage before the SPR took ownership of them in 1981. Cavern 3 was eventually filled with brine, plugged and abandoned. After that time, sixteen other storage caverns were created over a seven-year period. The analysis simulates the caverns that were leached to full size over some period of time and filled with brine until 1981 and then filled with oil. The analysis also simulates the leaching of the post-1981 caverns and subsequent filling with oil. In general, these caverns have been maintained at constant operating pressures except during workovers. The standard pressure condition applied to the cavern is based on an average wellhead pressure ranging between 900 and 975 psi. Beginning in the simulation year 1984, a series of five-year cycles of cavern workovers was initiated. During the five year cycle, every cavern is scheduled for a workover. During the workover, the affected cavern is held at 0 psi wellhead pressure for three months. The pressures for all caverns are at normal operating pressure for the fourth month (so that the workover rig can be moved to a new well) and then the workover of the next scheduled well begins. Previous analyses have shown that the abrupt pressure drop during the workover will induce the greatest potential for damage. The duration of the simulated workover may be slightly longer than is typically encountered in the field, but is chosen to provide an adverse condition and closely simulate actual subsidence measurements, which reflect periods of low to intermediate operating pressures associated with fluid transfers. After 2008, the simulation incorporates an additional feature. Each of the caverns is expected to experience five leaching operations to grow the cavern, with a volume growth of approximately 15% for each leach. (There are some exceptions to this: cavern 5 is not developed further due to its unwieldy shape; caverns 1 and 2 are leached only four times due to potential interference with other caverns; and cavern 113 is increased by 10% for each leach, also due to potential interference issues.) The leaching operations are simulated to begin in September 2008, which is the final four-month window in that particular five-year workover cycle. This is repeated in 2013, 2018, 2023, and 2028, and the calculation then performs one more workover for each cavern through 2033. Caverns 101-116 and 4 were meshed as axisymmetric caverns, using the average radius as function of elevation based on

sonar measurement data. Because of their highly non-cylindrical and asymmetric geometries, the meshes for caverns 1, 2, and 5 were created from extrusions based on a representative shape derived from the sonar data. (These three caverns also gained some nicknames due to their interesting shapes: cavern 1 is the "Potato", cavern 2 "Antarctica", and cavern 5 the "Toilet".)

In order to perform a cavern stability analysis that investigates damage in salt, the analytical tools ideally need to be able to perform the following functions: 1) calculate the changes in the in situ stress field and deformations surrounding the well and cavern over a long period of time due to the creep deformation of the salt; 2) include criteria by which tensile failure or shear damage of the salt can be determined and located; 3) have the ability to reduce the time step of the analysis to discretize short-time events such as changes in cavern pressure due to workovers; and 4) allow post-processing to be able to identify high strain and failure regions and compute volume changes. The computational models utilized the finite element code JAS3D (ideal for simulations of processes occurring over many years), the power law creep model for salt, and the half-dome computational mesh.

3.2 STRATIGRAPHY AND COMPUTATIONAL MESH

The original mesh developed for the computational model is illustrated in Figures 7 and 8. (For reasons which will be explained later in Section 3.4, this was not the final mesh used; however, this mesh can be used for illustrative purposes.) This mesh simulates the entire salt dome geometry. Figure 7 shows the entire mesh used for these calculations, and Figure 8 shows the same view with the overburden and surrounding rock removed to expose the caprock and salt formations. This mesh contained 5.4 million elements. Four material blocks are used in the model to describe the stratigraphic layers: the overburden, caprock, salt dome and the rock layers surrounding the salt dome. The overburden is made of sand, and the caprock layer is made of gypsum or limestone. The rock layers surrounding the salt dome comprised several layers of sandstone and shale; they have been modeled as one large layer of sandstone due to the minimal deviation in densities and rock mass moduli throughout those layers. The overburden and caprock thicknesses are reasonably constant over the entire salt dome, so for meshing purposes they have been given constant values (Neal et al., 1994); the overburden layer is 760 feet thick, and the caprock 280 feet thick. The post-1981 caverns were typically constructed on 750-feet center-to-center spacings. Table 1 lists the cavern coordinates, top-of-cavern depths, and initial heights and volumes used in the analysis. The coordinates are based on Texas field coordinates, and converted to mesh coordinates with Cavern 1 at the origin, and coordinate axes aligned with compass directions (X-axis for W-E, Y-axis for N-S).

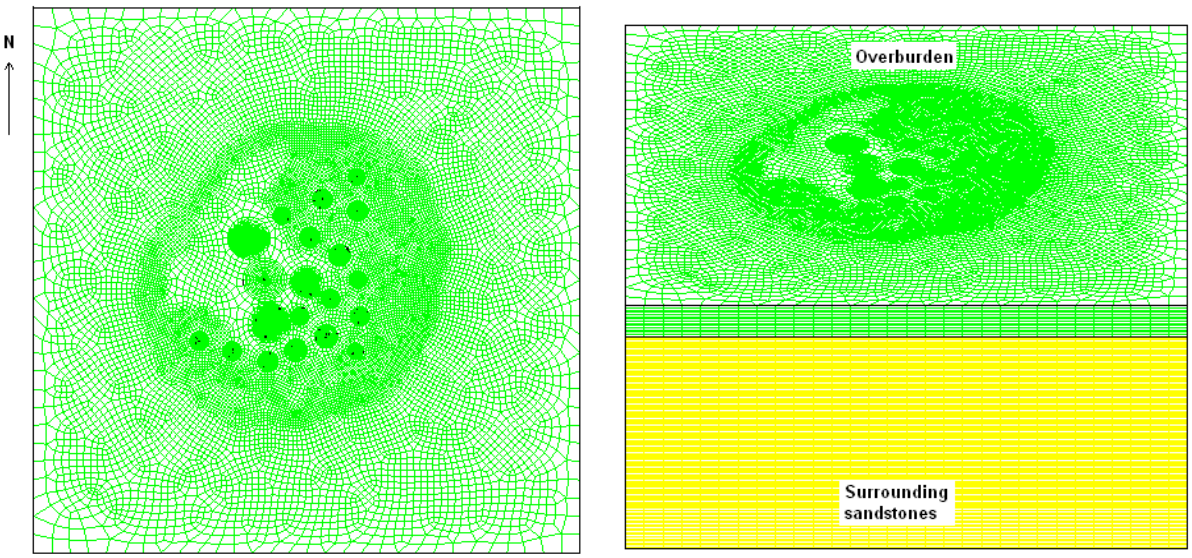

Figure 7. Original computational mesh developed for the Bryan Mound calculations.

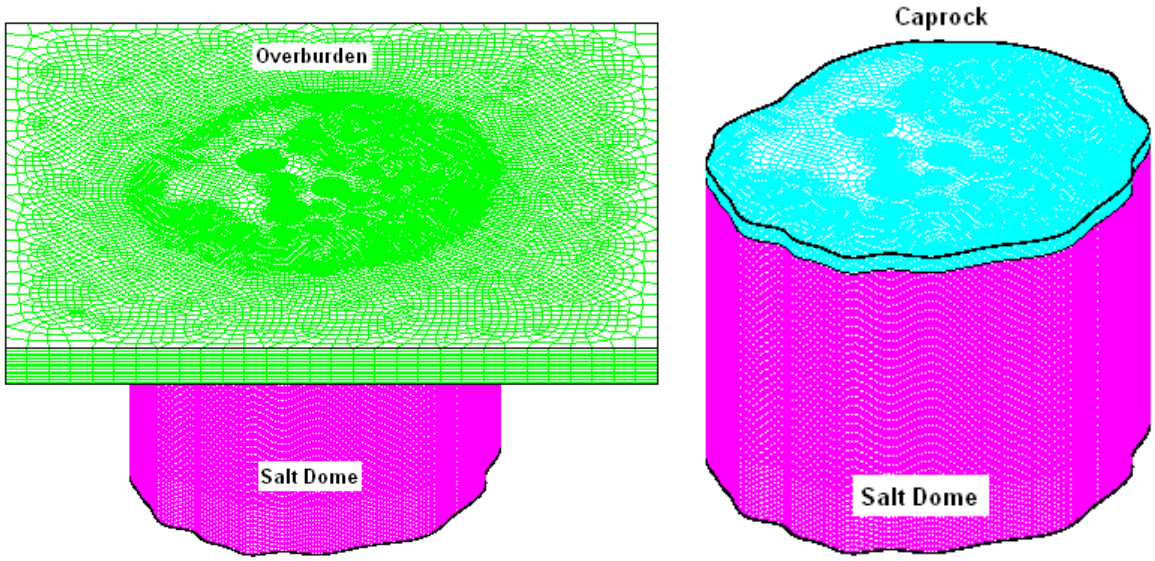

Figure 8. Original computational mesh showing the salt formation and sandstone.

Table 1. Cavern coordinates, depths, heights, and construction dates.

Bryan Mound Cavern	X, feet (positive X is West)	Y, feet (pos. Y is North)	Depth to Ceiling, feet	Initial Height, feet	Initial Volume, MMB (1993)	Begin Construct (approx)	End Construct (approx)	Begin Oil Storage (approx)
1	0	0	2349	413	8.46	1/1/1946	1/1/1947	10/1/1978
2	-829.881	-988.094	1450	220	6.32	1/1/1946	1/1/1947	2/1/1978
4	-904.481	23.80583	2495	581	20.68	1/1/1946	1/1/1947	1/1/1978
5	-1334.58	924.5058	2102	1171	37.87	1/1/1957	1/1/1958	1/1/1984
101	-546.781	1415.506	1998	2161	11.23	9/1/1982	9/1/1984	9/1/1984
102	347.2786	1785.598	2203	2034	11.52	1/1/1981	5/1/1984	5/1/1984
103	1116.697	1518.731	2122	2011	11.43	5/1/1982	5/1/1984	5/1/1984
104	70.43307	942.4114	2108	2055	11.7	1/1/1981	1/1/1983	1/1/1983
105	716.3358	544.0781	2050	2143	11.39	1/1/1981	7/25/1983	7/25/1983
106	1165.614	-800.839	2106	1905	12.45	1/1/1981	1/1/1983	1/1/1983
107	518.3775	-412.311	2150	1947	11.4	1/1/1981	1/1/1983	1/1/1983
108	1121.391	5.522499	2166	1964	12.17	9/1/1983	9/1/1985	9/1/1985
109	426.9886	-1245.69	2132	2044	11.57	7/1/1981	7/25/1983	7/25/1983
110	-153.281	-807.794	2140	1982	11.42	1/1/1981	1/1/1983	1/1/1983
111	1095.296	2266.909	2130	1998	11.21	1/1/1983	3/1/1984	3/1/1984
112	-241.881	-1550.89	2065	2040	10.98	12/2/1982	11/30/1984	11/30/1984
113	1066.019	-1562.79	2134	2066	7.07	1/1/1984	10/31/1985	10/31/1985
114	-856.484	-1799.09	2130	2036	8.23	8/1/1985	8/1/1987	8/1/1987
115	-1642.52	-1571.86	2146	1984	10.32	9/1/1984	8/1/1986	8/1/1986
116	-2359.92	-1338.53	2100	1845	10.74	8/1/1984	8/1/1986	8/1/1986

Figure 9 shows three views of the layout of the meshed caverns used for these calculations: a view showing their placement within the salt dome, and plan and elevation views of the caverns. Figure 10 shows the caverns with at their current volumes plus five additional extraction layers. The salt extraction layers, or onion skins, represent the proposed additional salt leaching operations to grow the existing Bryan Mound caverns. For this analysis, the first leaching operation was scheduled for September 2008, with each subsequent leaching at five-year intervals afterward. Two types of cavern realizations are included in this computational domain. Most of the caverns (101 through 116 and 4) are represented as axisymmetric caverns with the radius at each elevation based on the average radius obtained from the cavern sonar measurements, with five surrounding layers representing the five additional leaches to grow the caverns in the future. Caverns 1, 2, and 5 were created by estimating an average shape of the cavern at one or more elevation intervals and vertically projecting that shape. Caverns 1 and 2 required just one extrusion, and four onion skins were added to their meshes. Cavern 5, because of its unusual shape, required the construction of four distinct sections of the cavern, and the analysts decided not to attempt enlarging it due to potential meshing caused numerical instabilities as well as the likely impracticality of actually enlarging cavern 5 in the field. Each onion skin, when deleted, adds about 15% to the volume of the caverns.

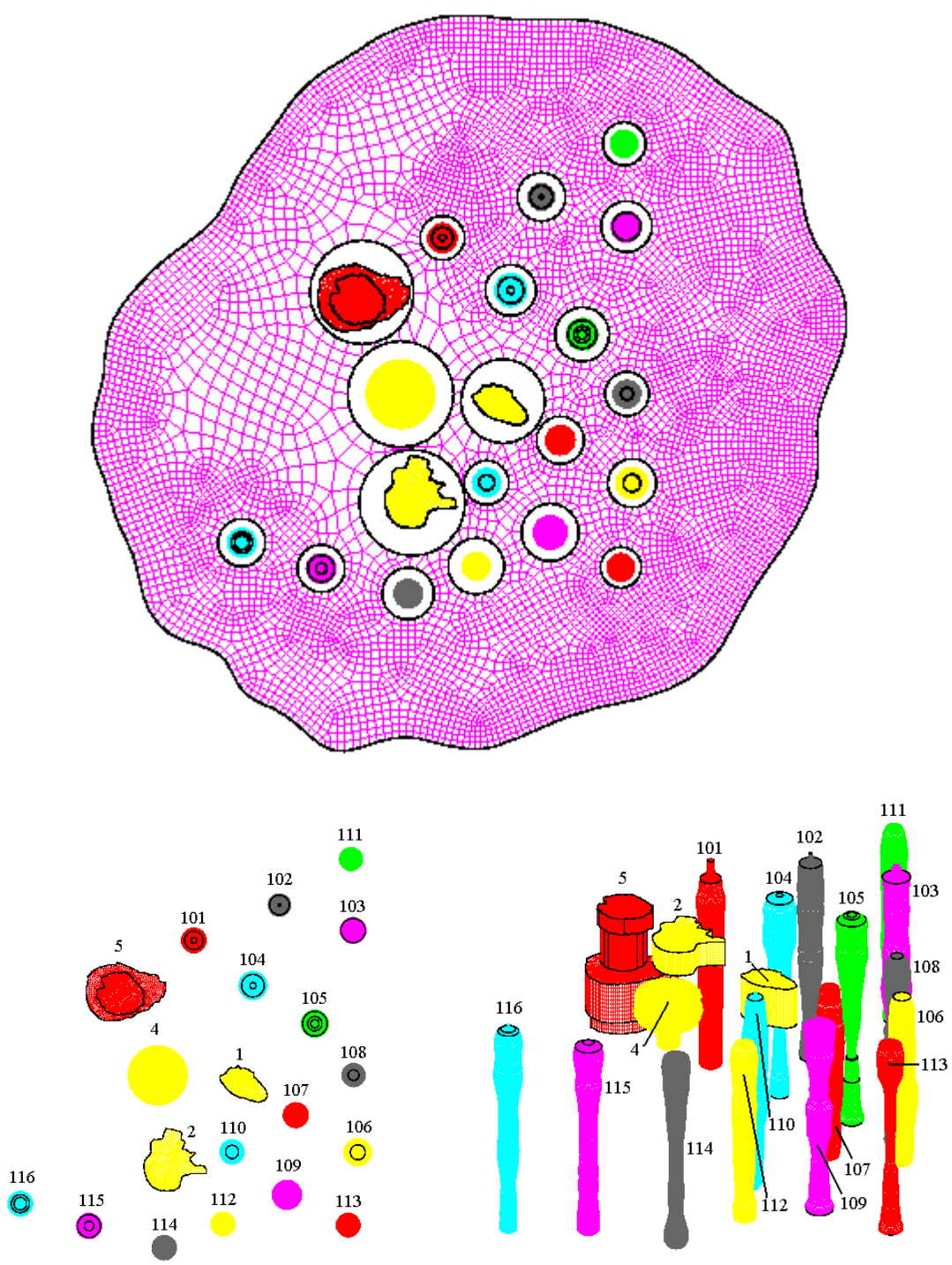

Figure 9. Bryan Mound caverns included in the original computational mesh (3 views).

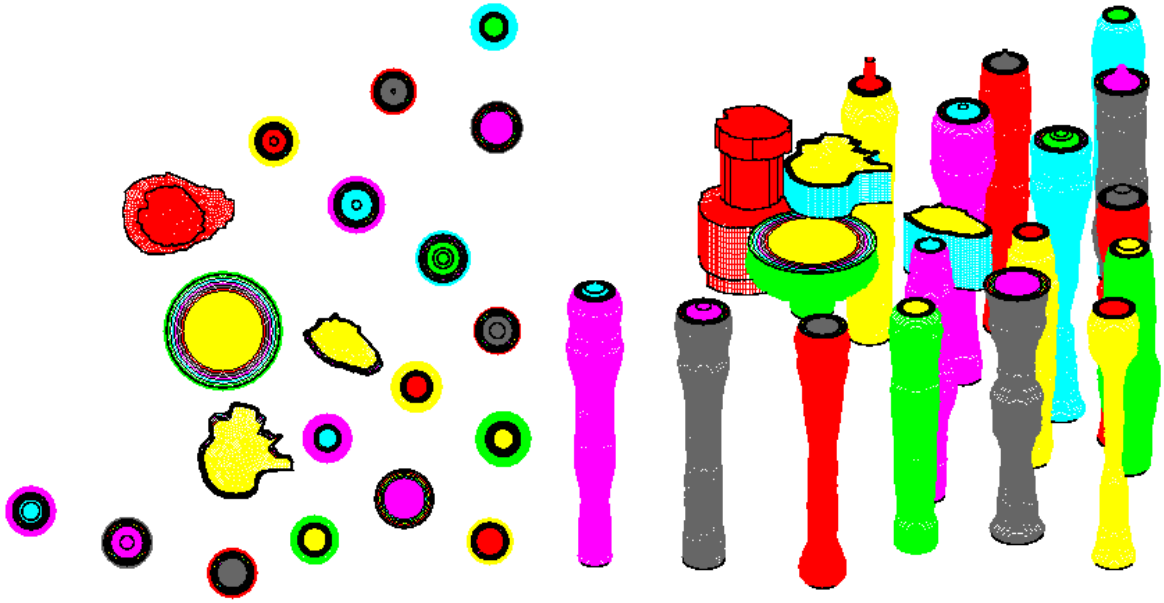

Figure 10. Bryan Mound caverns meshed with their additional extraction layers.

The other stratigraphic layers represented in the computational mesh include a 760 ft-thick layer of overburden modeled as a loose sandstone and a 280 ft-thick layer of caprock. The caprock and salt dome are surrounded by sandstone. These units are modeled with an elastic model much like previous SPR analyses. The addition of the surrounding sandstone allows for a better representation of the evolution of stress in the salt dome compared to that used in Ehgartner and Sobolik (2002), for which the 30-degree wedge included an infinite salt dome. The salt dome geometry was modeled after the results presented in Stein and Rautman (2005), and is to date the most realistic representation of an actual salt dome geometry used in a finite element analysis for SPR.

3.3 NUMERICAL AND MATERIAL MODELS

This analysis utilized JAS3D, Version 2.0.F (Blanford et al., 2001); a three-dimensional finite element program developed by Sandia National Laboratories, and designed to solve large quasi-static nonlinear mechanics problems. Several constitutive material models are incorporated into the program, including models that account for elasticity, viscoelasticity, several types of hardening plasticity, strain rate dependent behavior, damage, creep, and incompressibility. The continuum mechanics modeled by JAS3D are based on two fundamental governing equations. The kinematics are based on the conservation of momentum equation, which can be solved either for quasi-static or dynamic conditions (a quasi-static procedure was used for these analyses). The stress-strain relationships are posed in terms of the conventional Cauchy stress.

The power law creep model has been used for Waste Isolation Pilot Plan (WIPP) and Strategic Petroleum Reserve (SPR) simulations for many years. This creep constitutive model considered only secondary or steady-state creep. The creep steady state strain rate is determined from the effective stress as follows:

$$\dot{\varepsilon} = A(\sigma)^n \exp\left(-\frac{Q}{RT}\right), \quad (1)$$

where, $\dot{\varepsilon}$ = creep strain rate,

σ = effective or von Mises stress,

T = absolute temperature,

A, n = constants determined from fitting the model to creep data,

Q = effective activation energy,

R = universal gas constant.

The salt creep properties assume a homogeneous material, and are generally obtained from laboratory measurements. Values for the creep constant, the stress exponent, and the thermal activation energy constant for the power law creep model have been obtained for hard and soft salts through mechanical property testing of salt cores collected from boreholes (Munson, 1998).

3.4 MATERIAL PROPERTIES

It is desirable in large geomehcanical calculations to use salt properties that have been obtained through both laboratory experiments and through corroboration with measured field data such as cavern closure and surface subsidence. Laboratory values for SPR salts in Munson (1998) identify the West Hackberry and Big Hill salts as "soft" salts, and Bayou Choctaw and Bryan Mound as "hard" salts. For the West Hackberry site, these properties were further calibrated by numerical analysis to match the measured cavern closure and surface subsidence rates at the site (Sobolik and Ehgartner, 2007) by modeling half of the salt dome with surrounding sandstone. The West Hackberry analysis found that an increase to the creep coefficient A listed in Munson (1998) by a factor of 4 produced excellent agreement between predicted and measured surface subsidence and cavern closure. The current analysis models the entire Bryan Mound salt dome and all twenty caverns with specific geometries, and a similar comprehensive comparison between measured cavern closure and surface subsidence data has been performed.

Several sets of salt creep properties were used in calculations to compare with Bryan Mound historical data: the Munson (1998) hard salt properties, which are based on laboratory measurements and are a baseline for the SPR project, and sets identical to Munson's except that the creep constant A has been increased by a factor ranging from 1.8 to 13 (the reasons for this set will soon become apparent). The baseline property set is listed in Table 2. Additionally, an elastic modulus reduction factor (RF) was used to simulate the immediate primary creep response that is not captured in the power law creep (i.e. secondary creep) model. In order to obtain agreement with the measured closure of underground drifts at the WIPP, a reduced modulus was initially used to simulate the transient response of salt (Morgan and Krieg, 1990). The RF is known to vary (Munson, 1998). Limited creep testing of SPR salts (Wawersik and Zeuch, 1984) showed considerable variability in creep rates (up to an order of magnitude difference). For the West Hackberry site (Ehgartner and Sobolik, 2002), a value for RF of 12.5 was determined by calibrating to match the measured closure and subsidence rates at those sites

through back-fitting analysis. For these analyses, the modulus values in Table 2 are obtained from the standard modulus values in Munson (1998) divided by a reduction factor of 12.5.

Table 2. Baseline power law creep mechanical properties for Bryan Mound salt (Munson, 1998).

Property	Munson (1998)
Density, lb/ft^3	143.6
Elastic modulus, lb/ft$^{2\,*}$	51.8×10^6
Bulk modulus, lb/ft^2	34.5×10^6
Poisson's ratio	0.25
Creep Constant A, 1/(psf^n-sec)	1.43×10^{-30}
Exponent n	5.0
Q, cal/mol	10000
Thermal constant Q/R, °R	9059

* - An elastic modulus reduction factor of 12.5 was used in the calculations.

Cavern volume closure information for Bryan Mound Caverns 101-116 and 1-5 were obtained for the years 1990-2007. The cavern volumes are calculated from pressure data using the CAVEMAN program (Ballard and Ehgartner, 2000), and are reliable representations of cavern volumes during the normal operating environments when the pressurized cavern is slowly closing due to creep. These closure histories were compared to analyses using average cavern pressures based on the actual wellhead pressure histories at each cavern, and several salt property sets varying only in the multiplier assigned to the Munson creep coefficient A. These property sets are listed in Table 3. For the first two cases, the creep multiplier was applied to the entire salt dome. Table 4 lists the measured cavern closure rate for each cavern, and the predicted closure rates using the specified creep properties. Note that there is a significant discrepancy between the predicted and measured closure rates for the caverns. The closure rates for caverns 106, 109, 113, 114, and 115, are significantly under-predicted; the closure rates for the remainder of the caverns are bundled much more closely together, and can be under- or over-predicted depending on the value of the creep coefficient. A glance at the wide distribution in cavern closure measurements indicates that the Bryan Mound salt is significantly more heterogeneous in its creep properties than the West Hackberry salt. The Bryan Mound salt creep properties in Munson (1998) were obtained primarily from samples from boreholes for caverns 107 and 108; these caverns are among those exhibiting the least cavern closure and the easiest to overpredict. Furthermore, there seems to be a cluster of caverns (106, 109, 113, 114, 115) located in the region to the south of the SW-NE trending shear boundary line shown in Figure 4 for which the cavern closure is decidedly greater than for the other caverns (with the notable exception of cavern 112). For these reasons, a new computational mesh was generated that divides the Bryan Mound salt dome into "hard" and "soft" sections, approximately along the shear zone boundary shown in Figure 4. This new salt dome mesh is shown in Figure 11. The caverns 106, 109, and 112 through 115 are in the soft salt section. New creep property sets were applied to each section of the dome; these sets are defined by Cases #3 and #4 in Table 4. Cavern 112 is a special case, as it is also among the caverns with the least closure; for Case #3, it is given the soft salt properties, but for Case #4, the cylindrical mesh surrounding cavern 112 is given the hard salt properties for that case. An examination of Table 4 indicates that using the hard salt creep multiplier from Case #4 of 1.8 produces a reasonably good match with the combined measured cavern closure for all the hard salt caverns. Case #4 provides an exceptionally good match for several individual caverns, including 5, 102, 104, 107, and 110. The soft salt caverns

(highlighted in bold print in Table 4) are much more difficult to match, as even among them there is a wide discrepancy in the amount of closure. Caverns 113, 114 and 115, in particular, appear to reside in more rapidly-creeping salt. The Case #4 creep multiplier of 13 does produce reasonably good agreement for cavern 106 and 109. Because of the highly heterogeneous nature of the measured behavior in Bryan Mound caverns, it is difficult to define creep properties that generate a sufficiently good match with that behavior. For this analysis, the properties of Case #4 in Table 4 have been utilized. A comparison of the calculated creep rates from the properties listed in Table 4 and the Munson properties is shown in Figure 12. Note how the soft salt properties are more comparable to the West Hackberry salt.

Table 3. Salt property creep coefficients used in parametric comparisons.

	"Hard" Section	"Soft" Section
Creep Coefficient for Hard Salt (i.e., Bryan Mound), Munson (1998), A_m, $(psf^5\text{-}sec)^{-1}$	1.43E-30	1.43E-30
Case #1: Entire Salt A=10*A_m	1.43E-29	1.43E-29
Case #2: Entire Salt A=4*A_m	5.72E-30	5.72E-30
Case #3: Hard Salt A=4*A_m, Soft Salt A=10*A_m	5.72E-30	1.43E-29
***Case #4: Hard Salt A=1.8*A_m, Soft Salt A=13*A_m**	**2.57E-30**	**1.86E-29**

* - These creep properties are used for the analyses in this report.

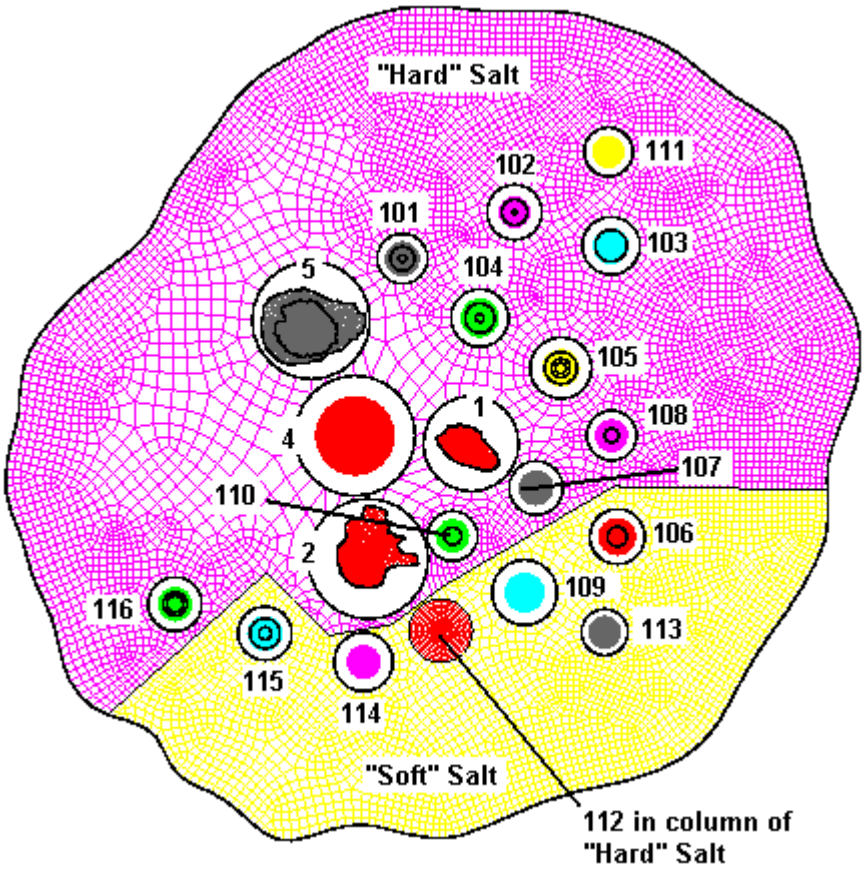

Figure 11. Computational mesh of the Bryan Mound salt dome with hard and soft sections.

Table 4. Measured and predicted cavern closure rates.

		Cavern closure rate, BBL/year, normal pressure range *			
Cavern	Measured closure	Case #1: Entire Salt $A=10*A_m$	Case #2: Entire Salt $A=4*A_m$	Case #3: Hard Salt $A=4*A_m$, Soft Salt $A=10*A_m$	Case #4: Hard Salt $A=1.8*A_m$, Soft Salt $A=13*A_m$
BM1	1,721	2,988	1,863	1,940	1,250
BM2	103	132	66	35	27
BM4	5,917	5,045	2,872	3,066	1,902
BM5	7,727	17,076	10,440	10,595	6,986
BM101	5,365	12,147	7,878	7,878	3,182
BM102	4,944	10,672	6,753	6,792	4,424
BM103	11,680	10,129	6,365	6,442	4,308
BM104	2,948	7,645	4,968	4,968	3,182
BM105	3,683	8,527	5,430	5,506	3,594
BM106	**10,460**	**9,300**	**5,884**	**8,683**	**9,063**
BM107	4,061	10,340	6,849	6,980	4,799
BM108	2,702	13,894	8,887	9,081	6,209
BM109	**8,543**	**9,431**	**6,054**	**9,198**	**10,051**
BM110	3,150	7,342	4,780	4,703	3,059
BM111	7,813	10,905	6,869	6,908	4,618
BM112	2,264	10,745	6,768	9,942	7,074
BM113	**10,223**	**6,462**	**4,015**	**6,271**	**6,959**
BM114	**21,304**	**9,120**	**5,705**	**8,654**	**9,120**
BM115	**21,034**	**9,081**	**5,550**	**8,383**	**8,732**
BM116	6,135	9,101	5,545	5,965	4,244
Entire site	141,778	180,082	113,539	131,991	102,785
Entire site except 106, 109, 113, 114, 115	70,214	136,688	86,331	90,802	58,859
Hard salt: Site except 106, 109, 112, 113, 114, 115	67,950	125,943	79,563	80,860	51,785
Soft salt: Caverns 106, 109, 113, 114, 115	**71,564**	**43,394**	**27,207**	**41,189**	**43,926**

* Creep coefficients for each case based on multiples of creep coefficient for hard salt (i.e., Bryan Mound), Munson (1998), A_m=1.43e-30 $(psf^5\text{-sec})^{-1}$

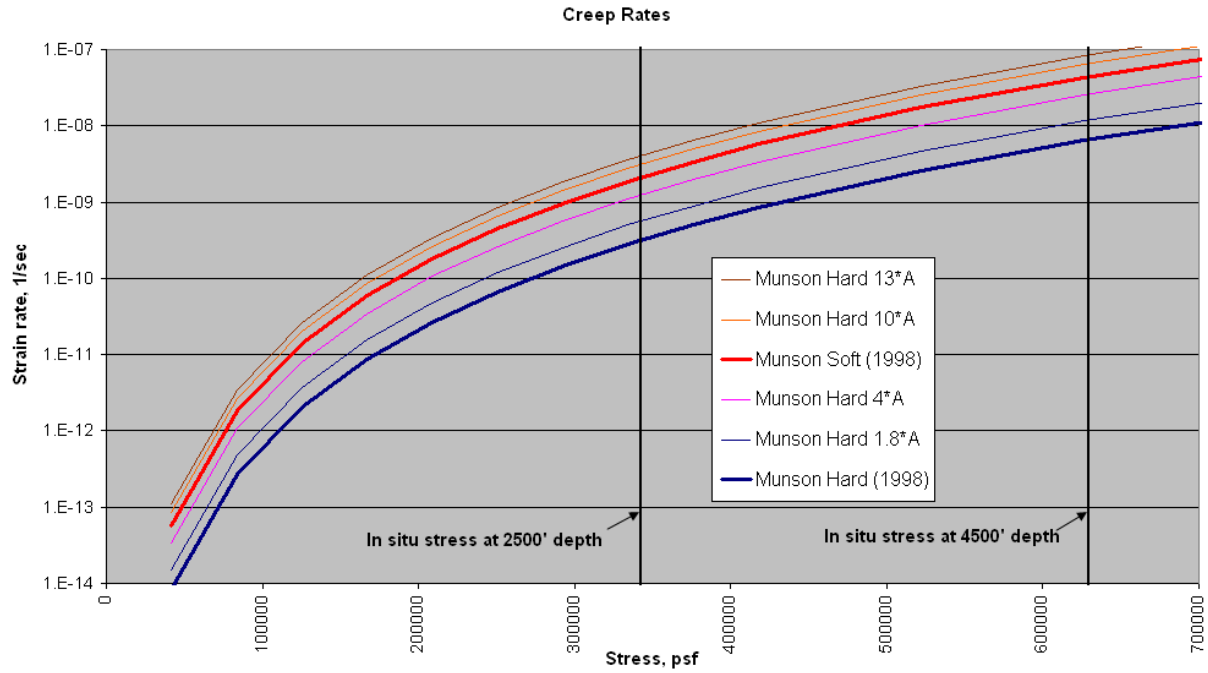

Figure 12. Calculated creep rates using different property sets.

The measured cumulative closure of the Bryan Mound caverns is plotted against predictions using the hard/soft salt creep properties of Case #4 in Figures 13 through 15. Figure 13 compares the caverns from the hard salt section for which reasonably good agreement was obtained. In comparing the measured and predicted results, it is important to look at the slope, or rate of change, of cavern closure, during the times of standard operations, where the applied wellhead pressure is approximately constant as is the resulting closure rate. The large changes in both the measured and predicted histories occur during large ΔP events, such as a workover. Note that for the predictions, there is a large increase in cavern closure at the beginning of the workover; this volume loss is partially recovered upon repressurization of the cavern. The ability to convert these large pressure changes to volume in the CAVEMAN routine is not well established, so the volume data do not indicate whether this large perturbation occurs during the workover. However, the measured volume is readjusted in CAVEMAN based on the amount of fluid removed during the workover, so the net volume change should be reliable. In Figure 13, note that both the closure rates during normal operating pressures, and the net volume changes through workovers, match reasonably well. Figure 14 shows measurements and predictions for caverns in the hard salt that do not match as well; again, this results from the apparent heterogeneity of the Bryan Mound salt. Figure 15 shows the same comparison for the caverns in the soft salt section; predictions for caverns 106, 109, and 113 are reasonably good, whereas those for caverns 114 and 115 severely underpredict their closure behavior.

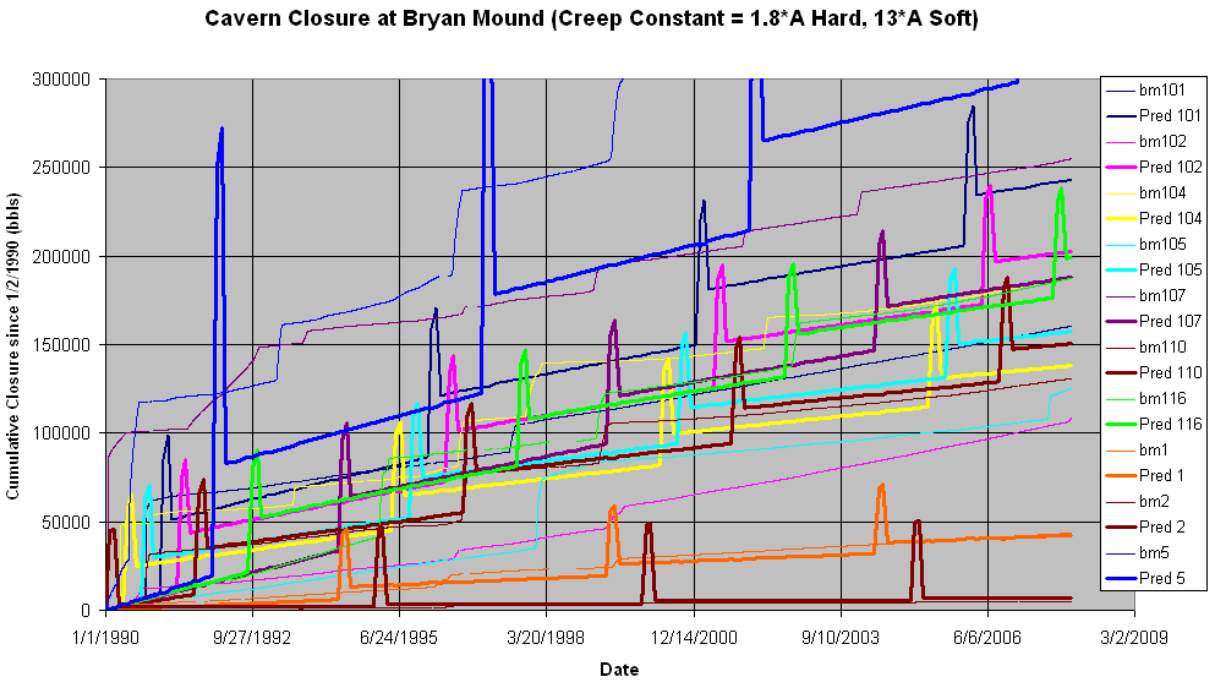

Figure 13. Cavern volume closure data, hard salt caverns, compared to predictions using developed Bryan Mound salt properties (good agreement).

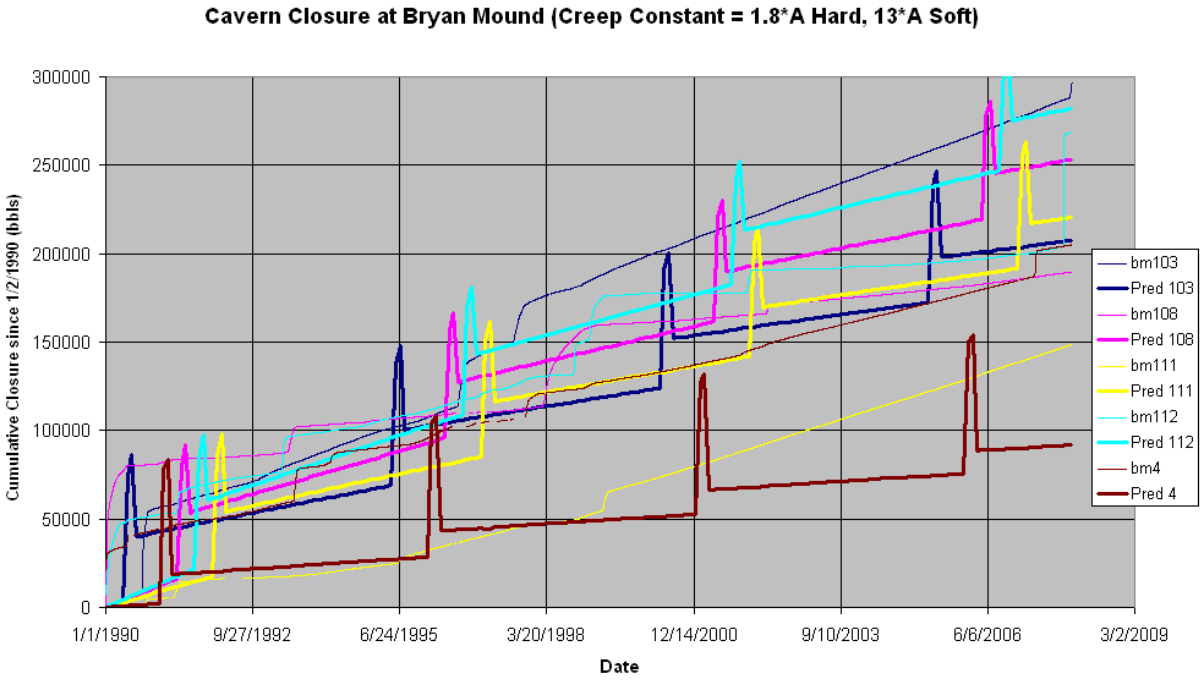

Figure 14. Cavern volume closure data, hard salt caverns, compared to predictions using developed Bryan Mound salt properties (lower quality agreement).

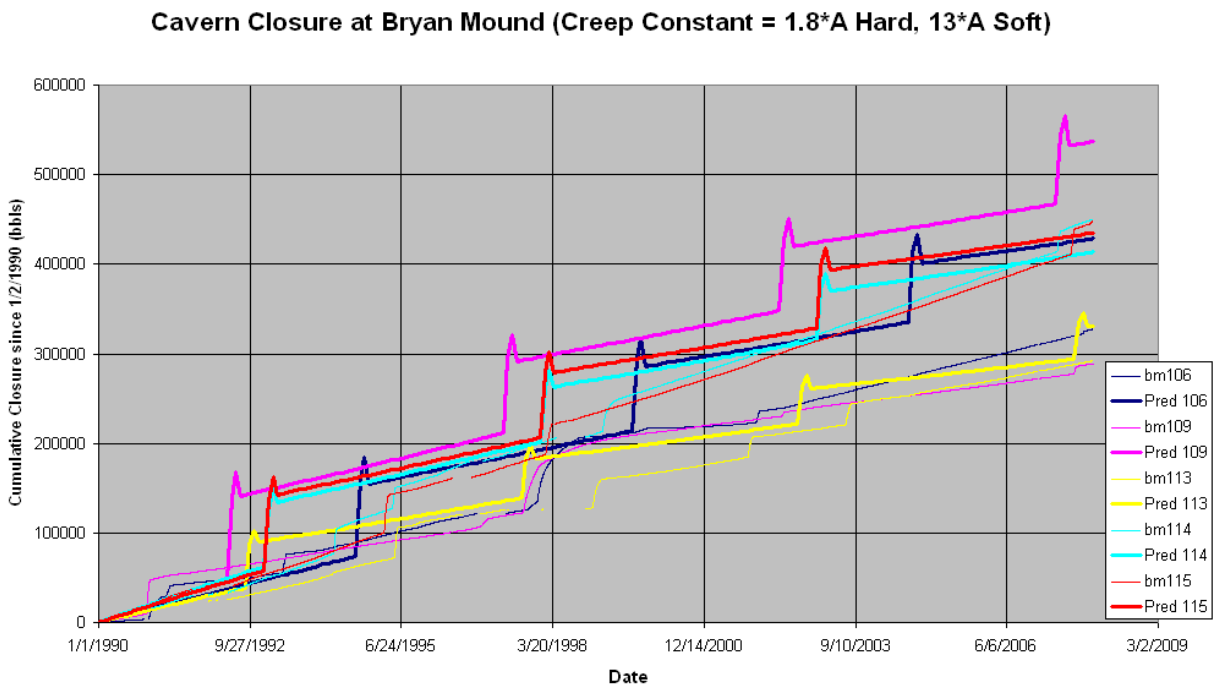

Figure 15. Cavern volume closure data, soft salt caverns, compared to predictions using developed Bryan Mound salt properties.

The other valuable measured parameter to use for the development of in situ salt creep properties is the measured surface subsidence. Measured surface elevation data over all twenty Bryan Mound caverns were obtained from March 1985 through January 1999 (Bauer, 1999). (Additional data were obtained after 1999, but nearly all the monuments used for elevation measurements were moved or replaced, making a continuous comparison before and after January 1999 difficult. The change in monument elevation causes the apparent reversal of subsidence for many of the locations plotted in Figures 16 and 17. However, the data through January 1999 are sufficient to make comparisons with model results. Also, the data for the monuments above caverns 113 through 116 were installed at a later date, and elevation data for those locations were not available until January 1992.) These data are easily converted to surface subsidence distances over the same period. Figures 16 and 17 show the measured subsidence data for caverns 101 through 116 in comparison with the Case #3 and Case #4 salt creep properties, respectively. The Case #3 properties actually provide a better match to the subsidence data than the Case #4 properties. In fact, the Case #4 properties tend to underpredict the cumulative displacements over the hard salt section by about 33%, and in the soft salt section by about 25%. Because the overall magnitude of surface subsidence is small (approximately 0.5 feet over 12 years), it was decided to use the Case #4 salt creep properties because of their better overall match of cavern volume closure. For a future analysis, it may also be advantageous to re-examine the caprock and overburden properties, as they certainly have an influence on the subsidence in the region.

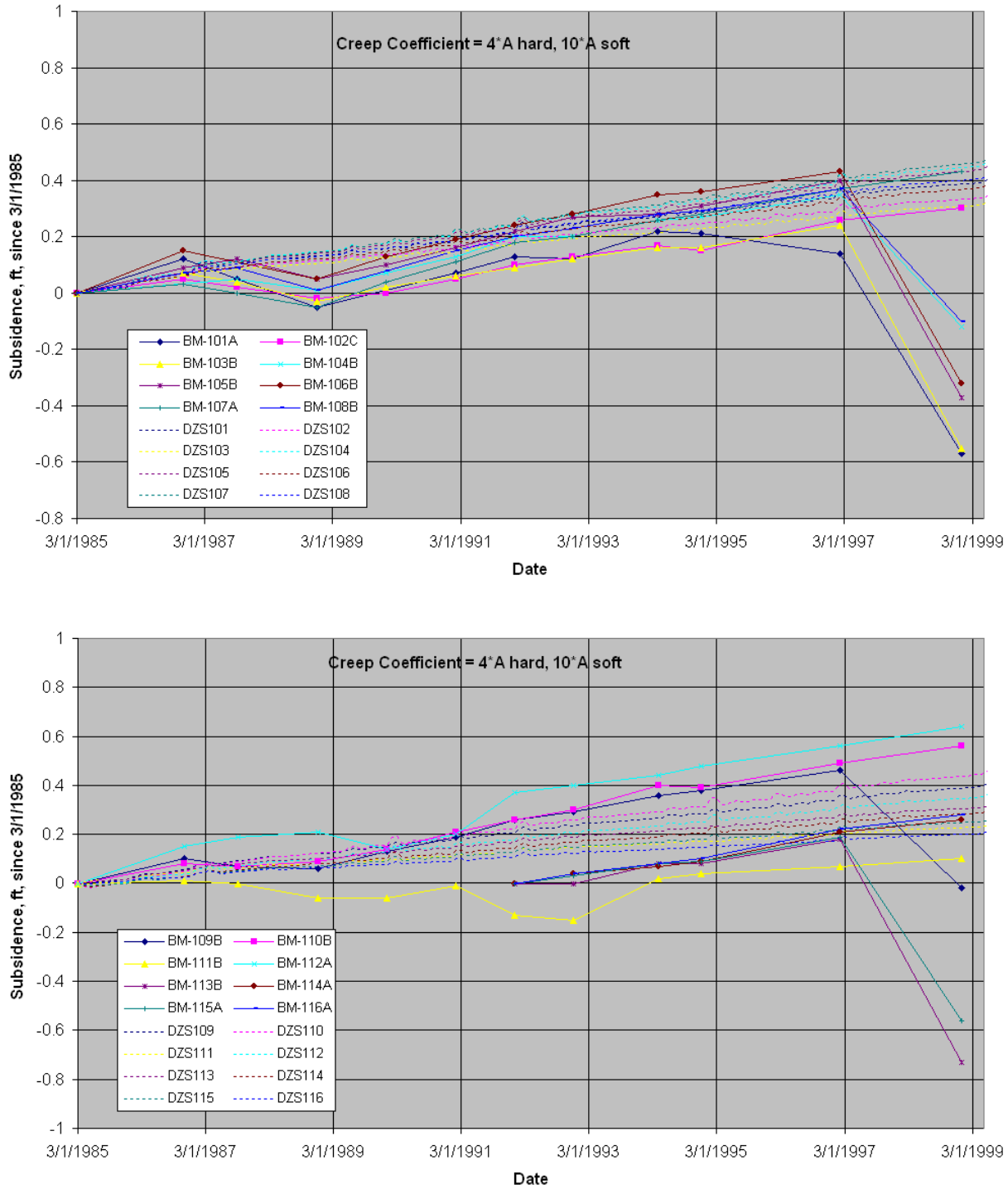

Figure 16. BM surface subsidence data for caverns 101-116, compared to predictions using Case #3 salt properties (dashed lines are predictions).

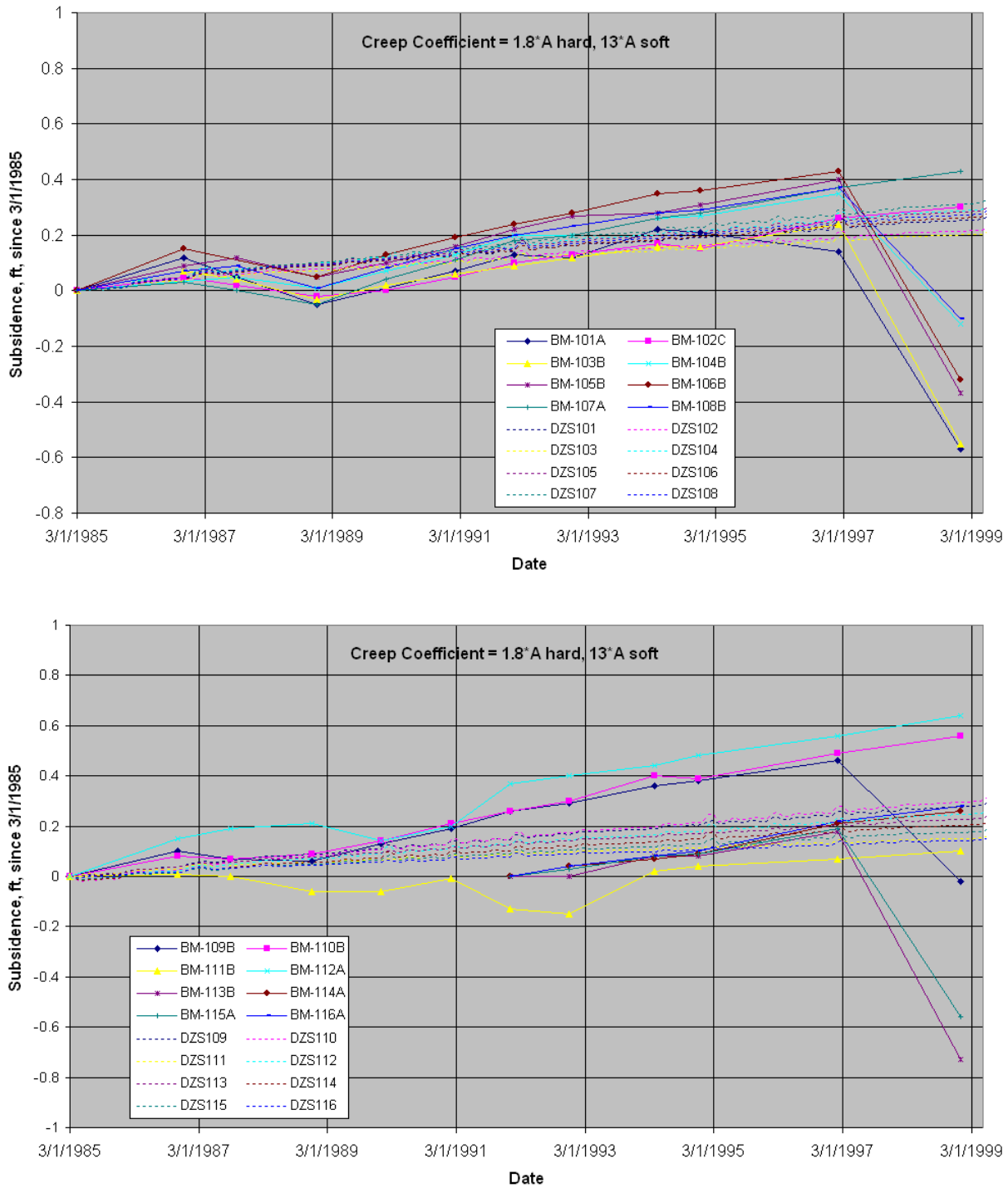

Figure 17. BM surface subsidence data for caverns 101-116, compared to predictions using Case #4 salt properties (dashed lines are predictions).

The surface overburden layer, which mostly comprises sand and sandstone, is considered isotropic and elastic, and has no assumed failure criteria. The caprock layer, consisting of

gypsum and limestone, is also assumed to be elastic. Its properties are assumed to be the same as those used for the West Hackberry analyses (Ehgartner and Sobolik, 2002). The sandstone surrounding the salt dome is assumed to be elastic (Lama and Vutukuri, 1978). Mechanical properties of each of these geologic materials used in the present analysis are listed in Table 5.

Table 5. Material properties of other geologic materials.

Parameters	Units	Overburden	Caprock	Sandstone
Density	lbm/ft^3	117.	156.	133.6
Young's Modulus	lb/ft^2	2.09×10^6	146×10^6	153×10^6
Poisson's Ratio		0.33	0.29	0.33

3.5 DAMAGE CRITERIA

The damage factor criterion (analogous to a safety factor) has been developed as a linear function of the onset of dilatant damage as a function of the hydrostatic pressure (Van Sambeek et al., 1993). Dilatancy is considered the onset of damage to rock resulting in increases in permeability. Dilatant damage in salt typically occurs at the stress state at which a rock begins microfracturing, causing an increase in the rock volume. Dilatant criteria typically relate two stress invariants: the mean stress invariant I_1 (equal to three times the mean stress) and the square root of the stress deviator invariant J_2, or $\sqrt{J_2}$ (a measure of the overall deviatoric or dilatant shear stress). (By convention, tensile normal stresses are positive, and compressive normal stresses are negative, hence the sign nomenclature in the following equations.) The dilatant criterion chosen here is the equation typically used from Van Sambeek et al. (1993),

$$\sqrt{J_2} = -0.27 I_1 . \qquad (2)$$

The Van Sambeek damage criterion defines a linear relationship between I_1 and $\sqrt{J_2}$, and such a linear relationship has been established from many suites of laboratory tests on WIPP, SPR, and other salt samples. This criterion was applied during post-processing of the analyses, using predicted stress states. A damage factor (safety factor) index was created (SF_{VS}) by normalizing I_1 by the given criterion:

$$SF_{VS} = \frac{-0.27 I_1}{\sqrt{J_2}} \qquad (3)$$

Several earlier publications define that the Van Sambeek damage factor SF_{VS} indicates damage when $SF_{VS}<1$, and failure when $SF_{VS}<0.6$. In previous studies, values of $SF_{VS}<1.5$ have been categorized as cautionary due to unknown localized heterogeneities in the salt that cannot be captured in these finite element calculations. This report will use these damage thresholds.

4. RESULTS

The historical performance of the Bryan Mound caverns, and their predicted future performance, will be evaluated on the basis of several design factors: dilatant and tensile stress damage to the salt surrounding the caverns, cavern volume closure, axial well strain in the caprock, and surface subsidence. These performance factors will provide metrics to determine the current condition of the caverns and their well casings, and the feasibility of expanding the storage capacity of the caverns.

4.1 DILATANT AND TENSILE STRESS DAMAGE NEAR THE PHASE 1 CAVERNS

There are two ways in which the salt surrounding the caverns can be damaged: by shear-stress induced microfracturing which increases permeability and the potential for crack propagation and by tensile stresses which causes salt tensile fracture and crack propagation. A quick way to evaluate the potential for damage is by the use of history plots of the extreme values of damage factor and maximum principal stress in the salt surrounding the cavern through each of the five leaching operations. Figure 18 shows the minimum value of the Van Sambeek damage factor (Equation 3) surrounding each of the twenty Bryan Mound caverns as a function of time. As stated in the previous section, lower values for damage factor indicate a higher likelihood for dilatant damage, with values <1.5 considered cautionary, values <1.0 indicating the onset of damage, and values <0.6 indicating failure of the salt, primarily in the form of substantial increase in permeability due to microcracking. In the computational mesh used for these analyses, each cavern and its subsequent "onion skins" removed at each leaching are surrounded by a cylinder of salt; the minimum value of safety factor plotted in Figure 18 is the minimum values within that cylinder and the existing onion layers at each time. The vast majority of the salt in each of the cylinders exists at very low deviatoric stress value, and thus very high values for the damage factor; only in the cavern walls and near vicinity are there sufficient deviatoric stresses to lower the damage factor significantly. The first modeled leaching operation occurs on 8/22/2008; in the calculation, the removal of a layer of salt is done to all twenty caverns simultaneously and instantaneously. Subsequent leaching operations occur at five-year intervals. Note that throughout the history of the caverns and their future expansions, the lowest values of damage factor occur during workover operation periods. For most of the caverns, the lowest damage factor reaches levels in the range of 1.2-1.5, which are in the cautionary range due to unknown heterogeneous conditions in the cavern walls. Figure 19 highlights five of the quasi-cylindrical caverns, 103, 104, 105, 110, and 113. Note that the lowest damage factor occurs for caverns in the middle of the hard salt area (104 and 105); the tendency is for salt with lower creep coefficients to react to pressure changes with larger deviatoric stresses. Cavern 103, also in the hard section of the salt, has generally higher values for the damage factor, possibly because it is among the boundary caverns; cavern 111 exhibited even somewhat higher factors. Cavern 113, located in the softer salt, tends to be least affected by workover pressure changes. Cavern 110, located in the hard salt but near the soft salt, performs somewhat better than caverns 104 and 105. Figure 20 shows a contour plot of a cross-section through cavern 104 during a workover; the location of the minimum damage factor occurs on the edge of the ceiling where it intersects the walls. (For all contour plots in this report, the positive x-axis points west, and the positive y-axis points north.) The critical locations for cavern 104 appear to be in the ceiling and around the perimeter about one-third of the elevation down from the ceiling, but there are no

significant concerns for this cavern. The other quasi-cylindrical caverns (101-116) exhibited similar behavior.

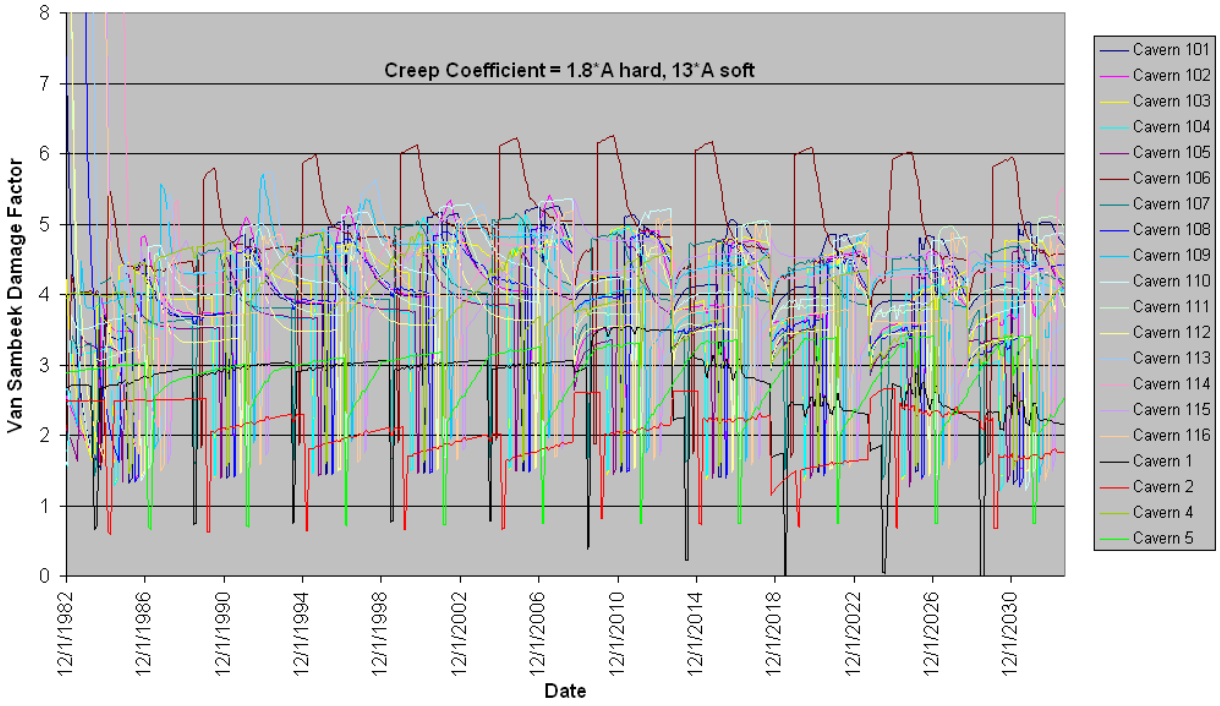

Figure 18. Minimum Van Sambeek damage factors from salt surrounding all Bryan Mound caverns.

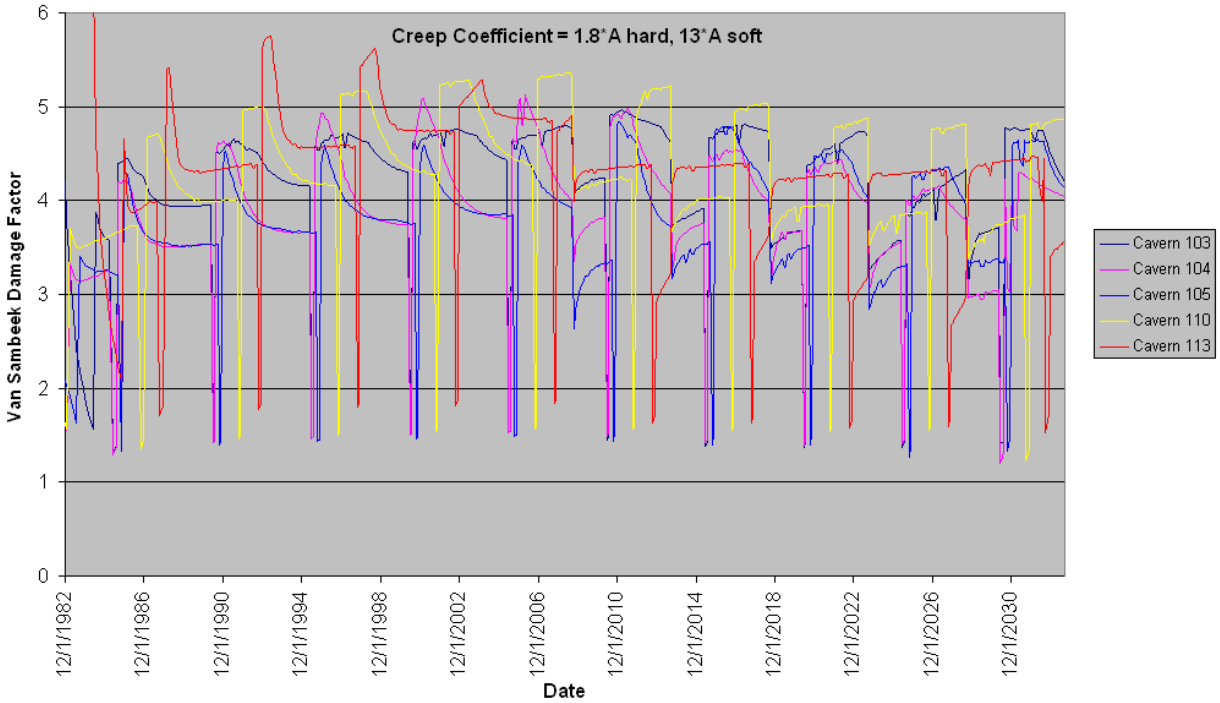

Figure 19. Minimum Van Sambeek damage factors from selected cylindrical cavern regions.

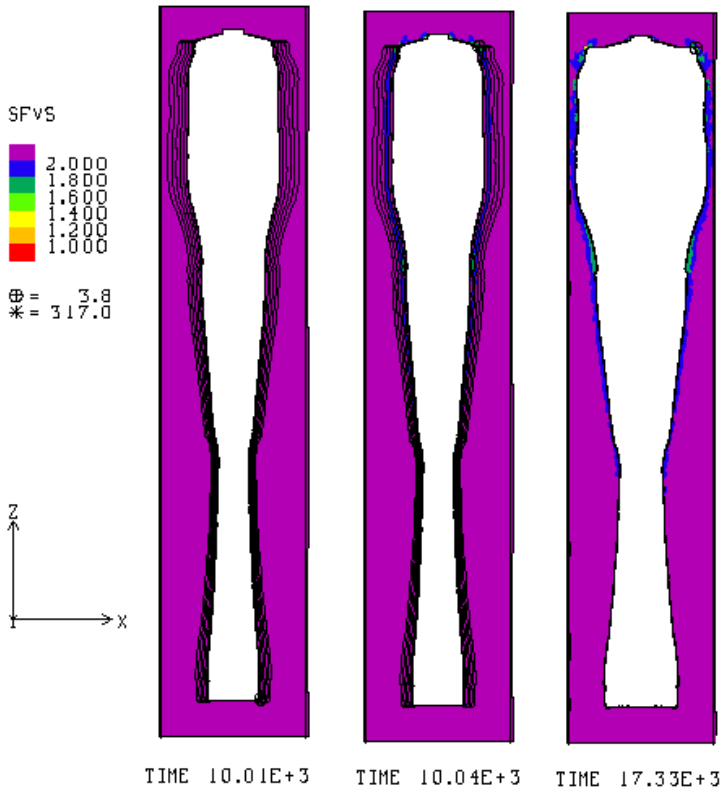

Figure 20. Contour plot of damage factor in salt surrounding cavern 104 during a workover.

In Figure 18, caverns 1, 2, and 5 all experience damage factors below 1.0 during workovers, with cavern 1 experiencing an alarming value of near 0. Figure 21 shows the minimum damage factor for just these three caverns. These three caverns have a much higher diameter-to-height ratio than the other caverns, so it is not surprising that they exhibit higher potential for dilatant conditions. As this is the minimum value, it is important to know whether the minimum values in Figure 21 are representative of a large area surrounding the caverns, or are anomalous spikes in an otherwise well-conditioned salt. Figure 22 shows the damage factor plotted in the layer of cells surrounding the vertical wall of cavern 1 before and after the initiation of a workover. The red cells indicate a damage factor less than 1.0. Before the workover commences, the walls are in satisfactory condition; once the pressure is decreased, bands of higher deviatoric stress occur around the perimeter near the ceiling and floor of the cavern, and small individual locations experience behavior in the damage domain. These locations tend to be in the ends of the cavern along the long elliptical diameter, and in regions where the cavern has a sharp edge jutting inward. The bottom view in Figure 22 shows three onion skin layers of cavern wall at this time, and this plot indicates that the extent on the damage zone does not go very far into the salt (each onion skin layer has variable thickness between 2.5 and 5 feet). Figure 23 shows the ceiling of cavern 1 at this time, and there are no regions of concern there. The analytical results suggest that there may be some minor damage in areas where the cavern geometry is not smooth, but predicts no large-scale regions of concern.

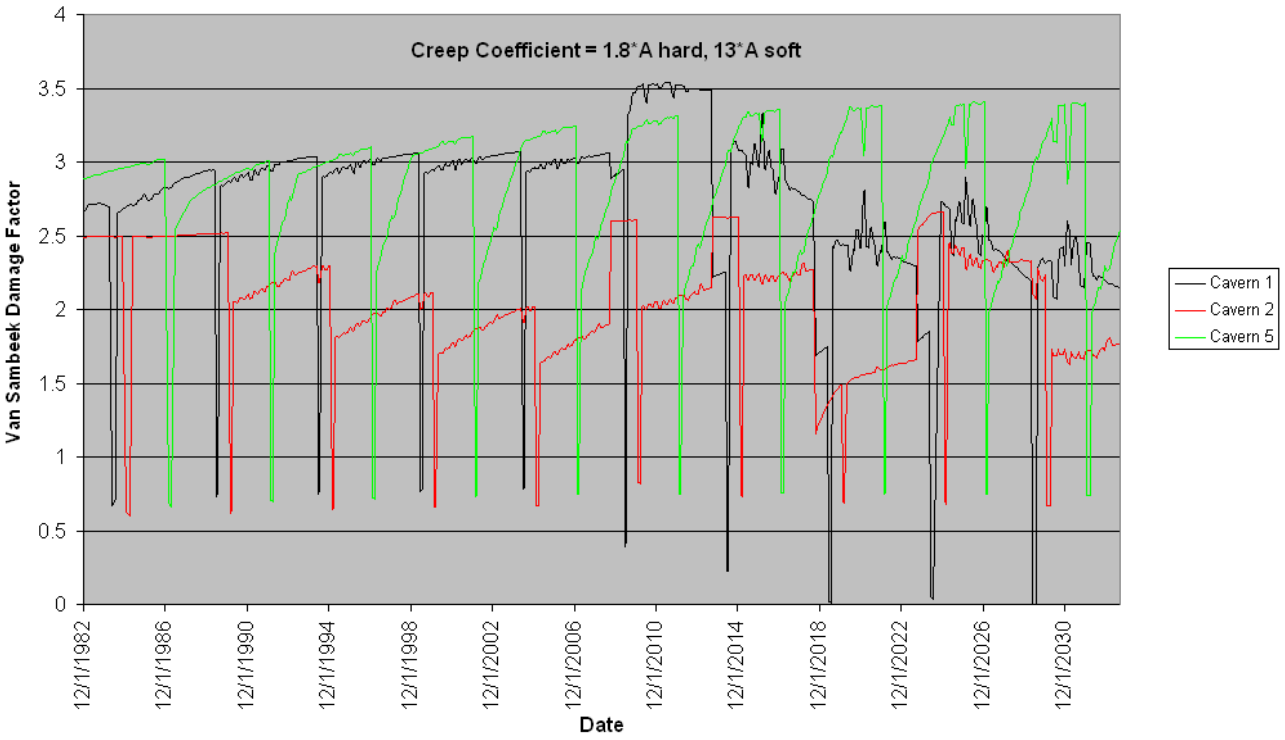

Figure 21. Minimum Van Sambeek damage factors near caverns 1, 2, and 5.

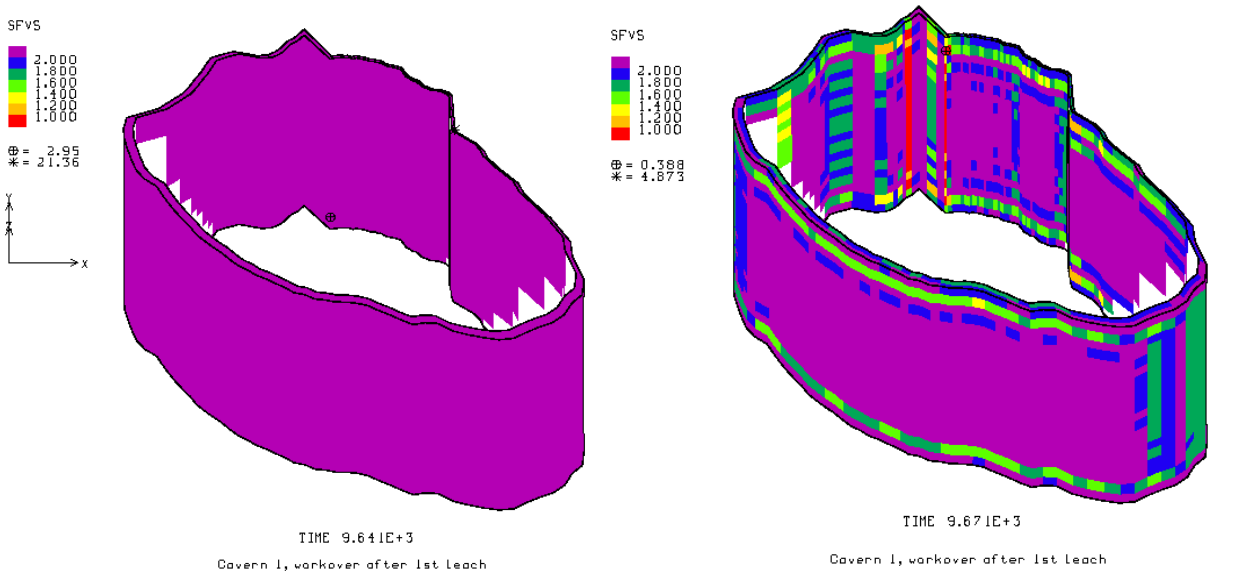

(a) Before workover

(b) During workover after pressure decrease

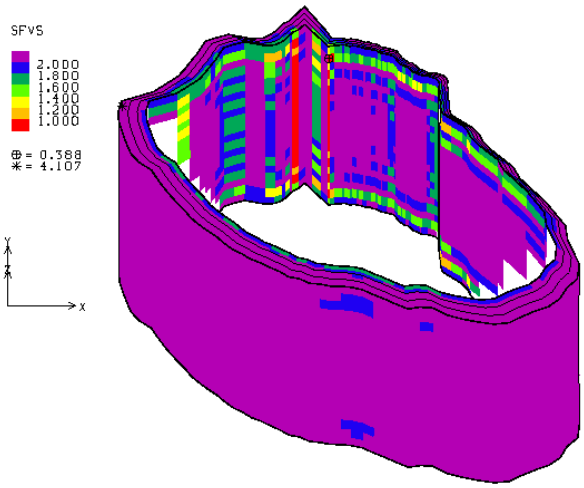

(c) During the same workover (showing three surrounding layers of salt)

Figure 22. Contour plots of damage factor in the salt in the walls of cavern 1 before and during a pressure decrease from a workover operation.

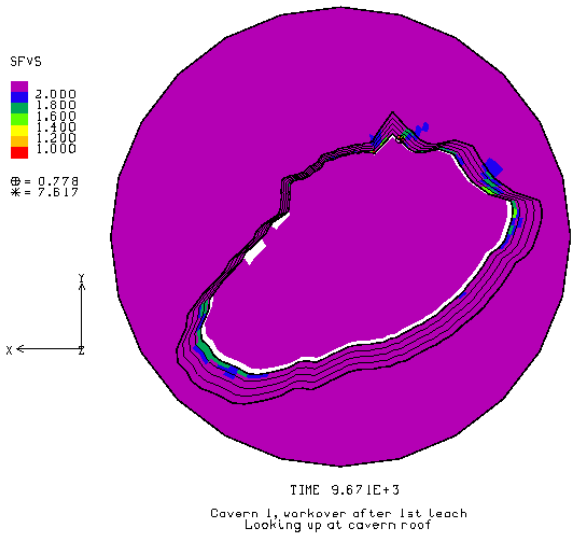

Figure 23. Contour plot of damage factor in the salt in the ceiling of cavern 1 after a pressure decrease from a workover.

Figure 24 shows a series of contour plots showing the damage factor around cavern 2 before and during a workover operation. Cavern 2 has a larger horizontal area than the other Phase 1 caverns, which would make salt damage a greater concern; however, the cavern benefits from being only about 220 feet tall and so close to the top of salt. Nearly the entire cavern wall experiences some prominent deviatoric stress, with sharp corners seeming to be the worst spots. Also, plot (d) in Figure 24 shows that the deviatoric stresses go further into the salt than they did for cavern 1. Figure 25 shows the distribution of damage factor in the ceiling during a workover following the first leaching; the ceiling appears to maintain satisfactory stress states. The results shown in Figures 24 and 25 are representative of the results following each successive cavern expansion. These results indicate that there is some potential for dilatant stress damage during workover periods, and the cavern should be monitored during such events. However, the analyses do not indicate any reasons not to expand cavern 2.

Due to its unusual geometry and its proximity to other caverns, cavern 5 was not meshed with additional onion skins for cavern expansion. Cavern 5 has two large lobes, one above the other, connected by a smaller neck between the two. The meshed version of cavern 5 is made from five cylindrical sections; however, it models the general character of the cavern. Figure 26 shows the damage factors in the salt surrounding cavern 5 in two cross-sections, during a workover. The area of concern is in the region of the neck, at the bottom of the top lobe and top of the bottom lobe. Dilatant damage in this section of the cavern may cause salt falls which would potentially strike casing strings passing through the neck; this may explain this cavern's history of casing failures. With the exception of the neck region, the remainder of the cavern does not appear to present significant concerns regarding potential salt damage.

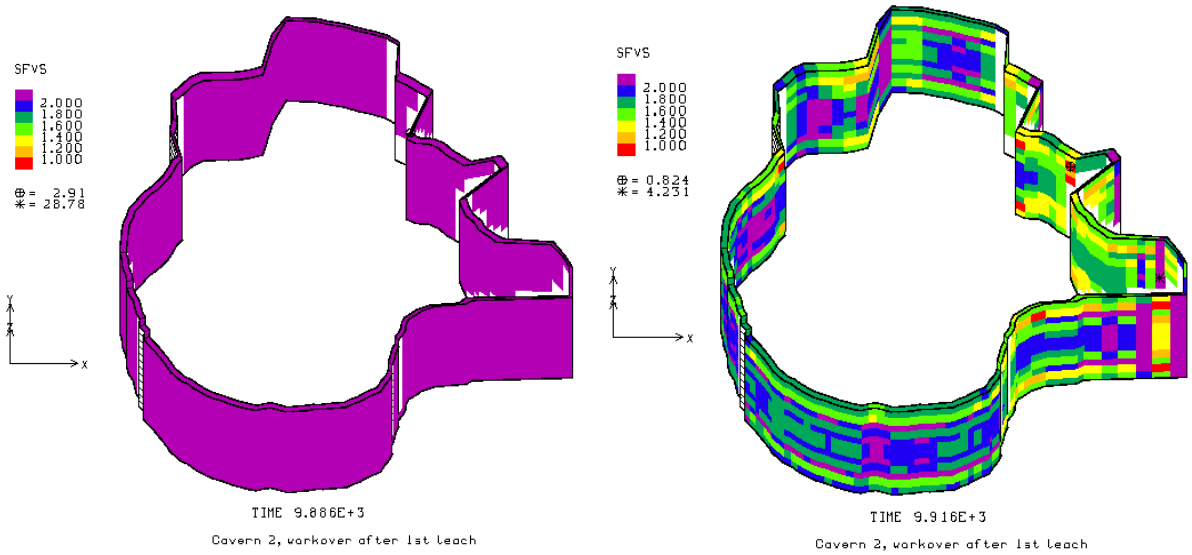

(a) Before workover (b) During workover

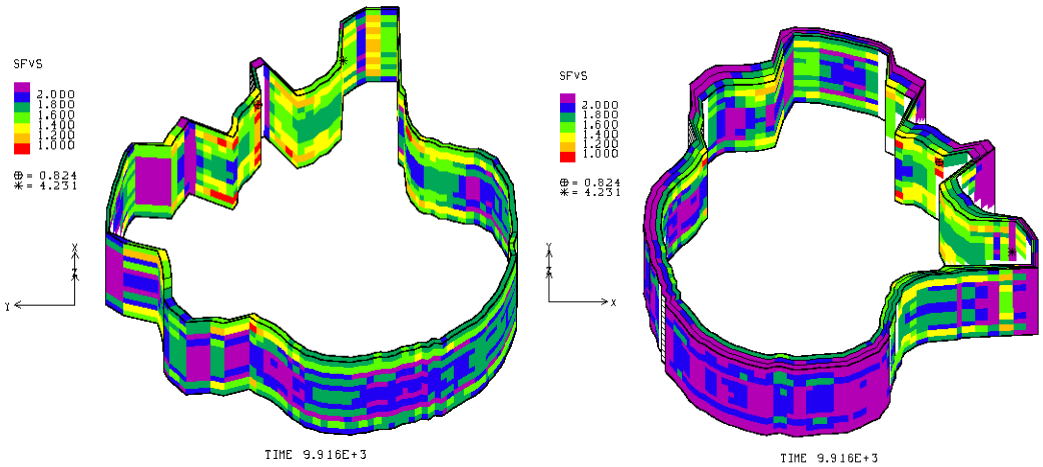

(c) Rotated view (d) Effect deeper into salt

Figure 24. Contour plots of damage factor in the salt in the walls of cavern 2 before and during a pressure decrease from a workover operation.

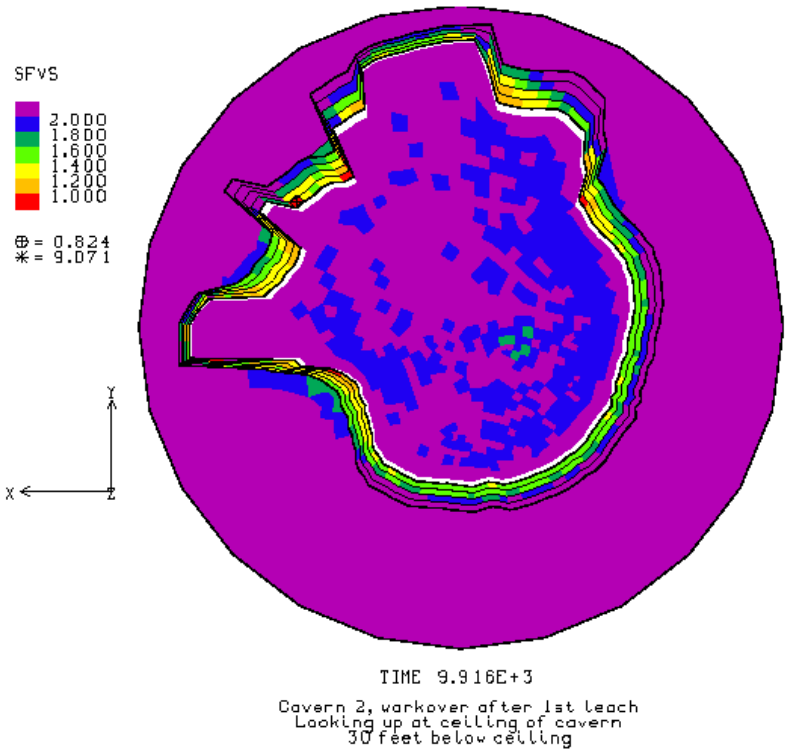

Figure 25. Contour plot of damage factor in the salt in the ceiling of cavern 2 after a pressure decrease from a workover.

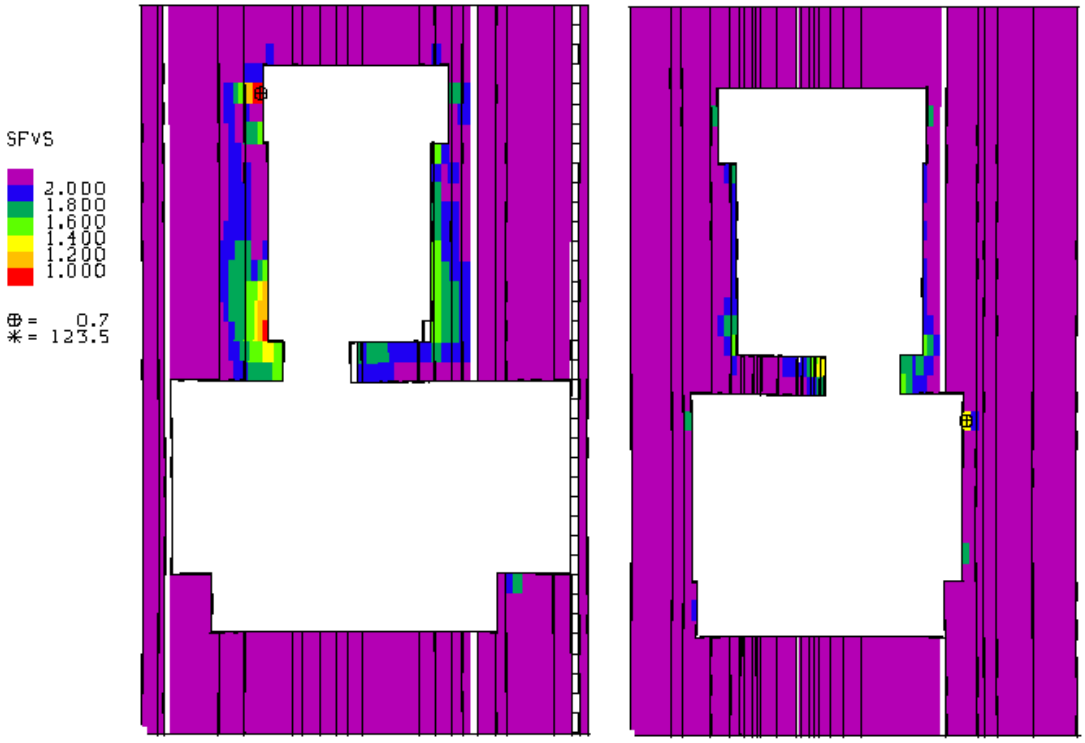

Figure 26. Contour plot of damage factor in the salt around cavern 5 (two cross-sections, looking north and west).

The other indicator of salt damage is the normal stress. Salt fractures under very low tensile stress (on the order of 1 MPa or 20,000 psf), so any indication of tension in the salt is of concern. Figure 27 shows the maximum normal stress in the salt surrounding each of the caverns. The maximum normal stress is determined from the maximum principal stress at each location in the salt. For all but three caverns, the normal stress remains negative, in the compressive regime. Again, caverns 1, 2, and 5 have peaks of tensile stresses during the workover operations. Figures 28, 29, and 30 show the locations of tensile stress for these three caverns. Note that they tend to be the same locations as the high deviatoric stresses identified by the low damage factors. These results, along with those from the damage factor plots, suggest that caverns 1, 2, and 5 may require special monitoring during workover operations. Cavern 1 appears to be the least problematic, as its areas of concern tend to be highly localized to areas with sharp-edged geometries. The perimeter of cavern 2 is its primary area of concern; monitoring of cavern pressure and volume is suggested here to determine if significant wall cracking and leakage has occurred. The primary problem with cavern 5 appears to be in the neck area, where salt falls may impact the casing strings.

According to several reports, casing failures at the Bryan Mound site tend to be concentrated in a few caverns: 5, 103, 106, 107, 108, 109, and 112. A potential cause for those in cavern 5 has already been established. Regarding the other caverns, a possible pattern can be detected. Caverns 106, 109, and 112 are located to the south of the shear boundary layer used to divide the salt dome in the computational mesh. Caverns 107 and 108, though north of the shear boundary, are close to it. Cavern 103 is well away from the shear boundary, but it also appears to be located in a soft subset of the dome based on its observed cavern closure behavior. It is possible that as the creep properties of the Bryan Mound salt are highly variable throughout the dome, so also may be the ultimate strength of the salt, and these variances may correlate with each other. The measured and computed results of this analysis suggest that the site properties of the Bryan Mound salt be reexamined for their variability and distribution throughout the dome.

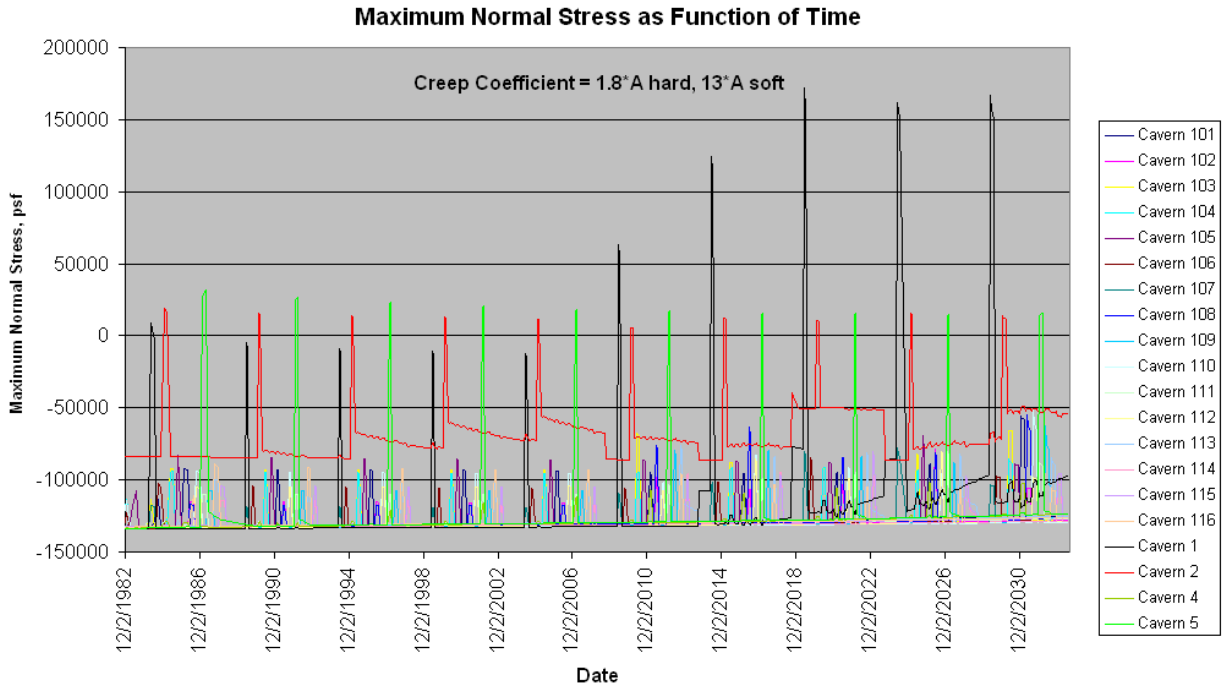

Figure 27. Maximum normal stress from salt surrounding all Bryan Mound caverns.

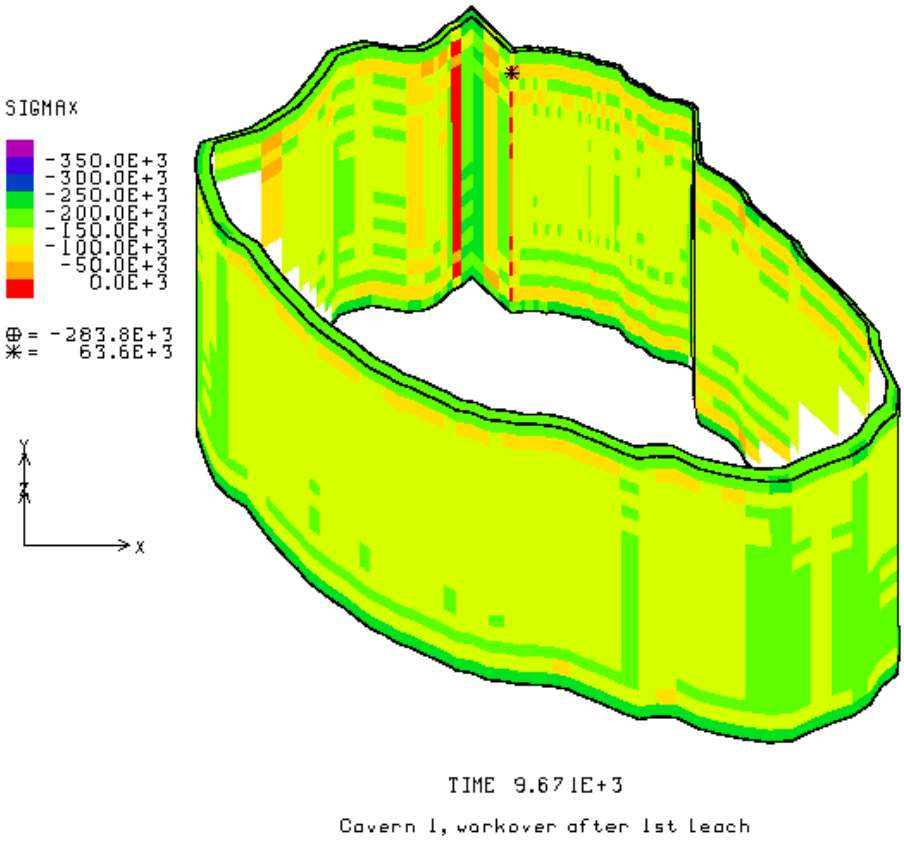

Figure 28. Contour plot of maximum normal stress (psf) surrounding cavern 1.

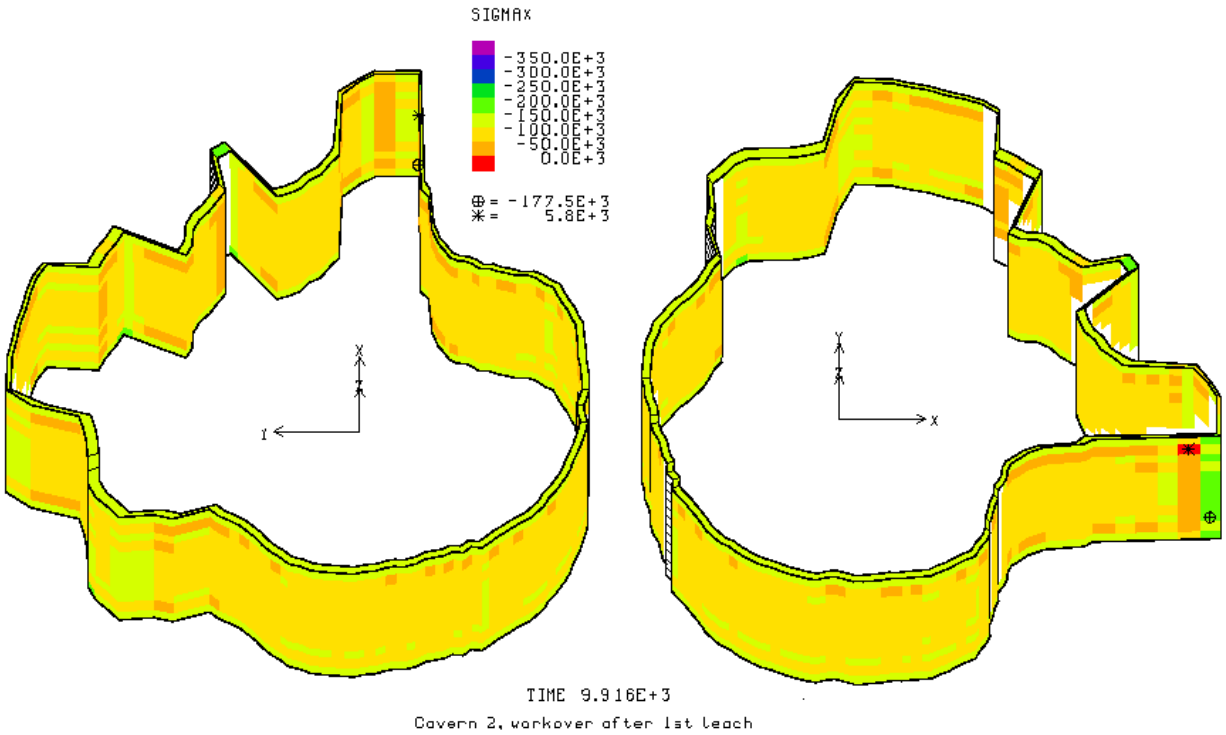

Figure 29. Contour plot of maximum normal stress (psf) surrounding cavern 2.

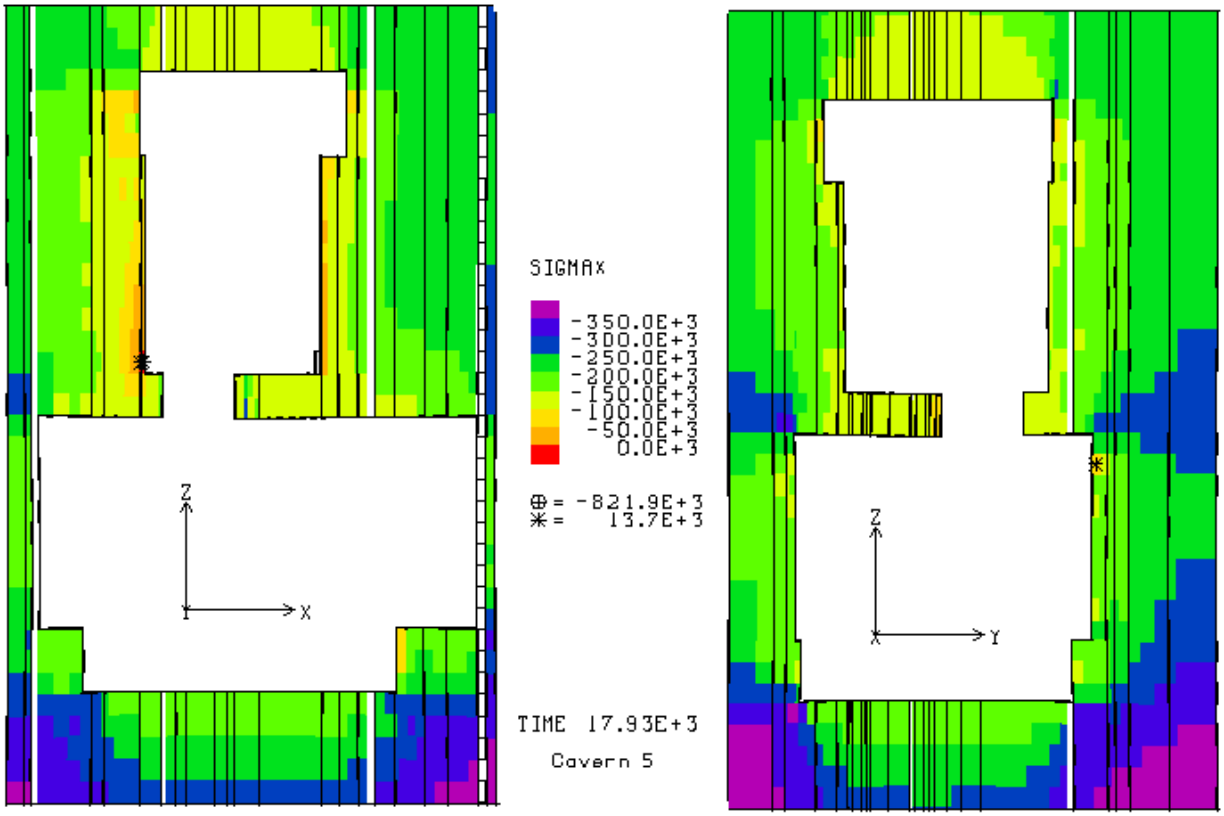

Figure 30. Contour plot of maximum normal stress (psf) surrounding cavern 5.

4.2 CAVERN VOLUME CLOSURE

The volume of the caverns decreases as the salts creeps. Figure 13 showed a good agreement between the predicted cavern closure rate and that measured for several of the caverns in the hard salt. Figure 14 showed predictions for some of the other caverns in the hard salt that did not match the measurements as well, and Figure 15 showed predictions for the caverns in the soft salt that had mixed success in matching the measurements. Predicted cavern closure up to the present, and into the future, depends upon the timing of workover operations, during which the caverns undergo their greatest deformation, and of future cavern expansion (leaching) operations. Figure 31 shows the predicted cumulative cavern closure for the hard salt caverns of Figure 13 based on a normalized volume. The normalized volume is the volume at a given time divided by the initial volume of each cavern for its given leaching cycle. For example, cavern expansion activities are forecast to begin in late 2008; when each cavern is expanded, a new initial volume is defined equal to the initial volume after leaching. Caverns 116, 101, and 102 experience the greatest cavern closure; there is no apparent pattern regarding cavern size, depth, or location to explain this ranking. Caverns 1, 2, and 5 experience the least closure because they are shallower than the other caverns, thus avoiding the higher stress differential between cavern pressure and in situ stress experienced at greater depths. The maximum net closure rate for these caverns is 0.018%/year, about an order of magnitude less than that for West Hackberry (Sobolik and Ehgartner, 2007). This point substantiates the notion that, on average, Bryan Mound is a hard salt, even though it has significant localized heterogeneities. Figure 32 shows the predictions for the other caverns in hard salt for which lower quality agreement with the measurements was reached (the caverns from Figure 14). According to the results in Figure 14, the predicted closure in Figure 32 for caverns 108 and 112 is significantly overpredicted, by perhaps a factor of 3. Similarly, the closures for caverns 4, 103, and 111 are underpredicted by factors ranging from 2 to 3. Figure 33 shows the results for the caverns located in the soft salt section. The predicted closures for caverns 113, 114, and 115, are shown in Figure 15 and Table 4 to represent underpredictions by a factor ranging from 1.6 to 2.4. Therefore, the volume closure rate could be as high as 0.12%/year for cavern 114. The predictions for caverns 106 and 109 in Figure 33 match the data reasonably well, and predict a closure rate of 0.041%/year. For all the cylinderically-shaped caverns, the majority of the volume loss occurs near the bottom of these caverns because of the greater stress differential at lower depths.

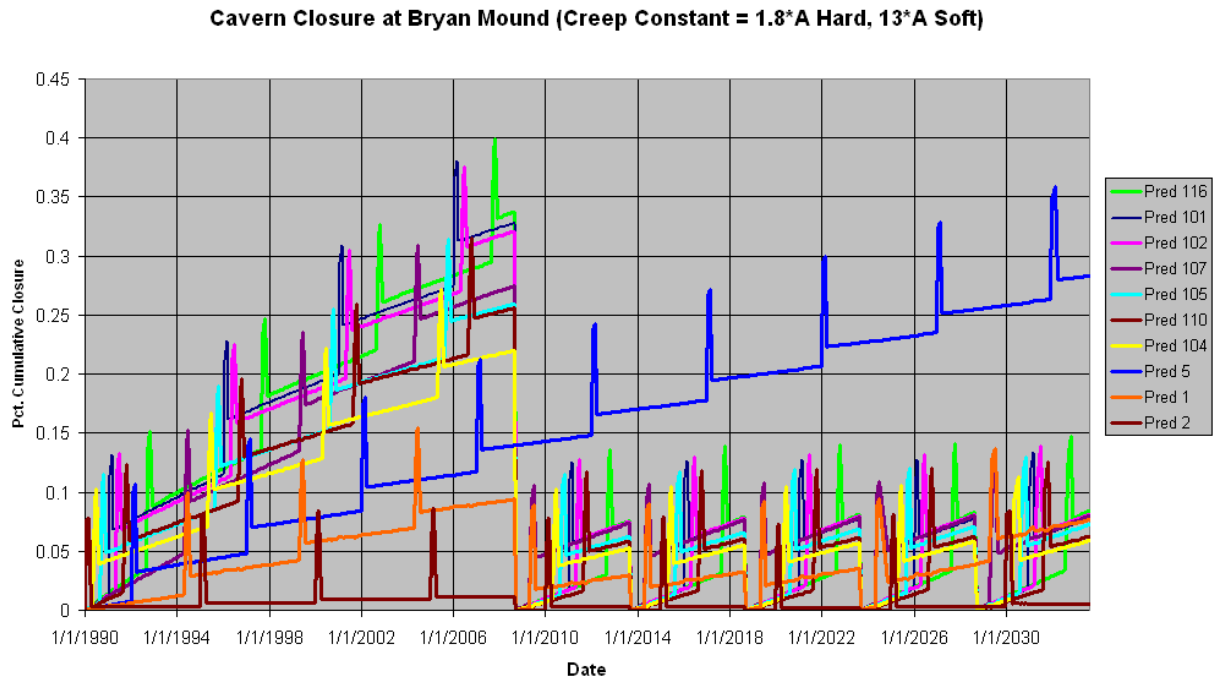

Figure 31. Predicted percentage closure of selected caverns in the Bryan Mound hard salt (corresponding to the caverns in Figure 13).

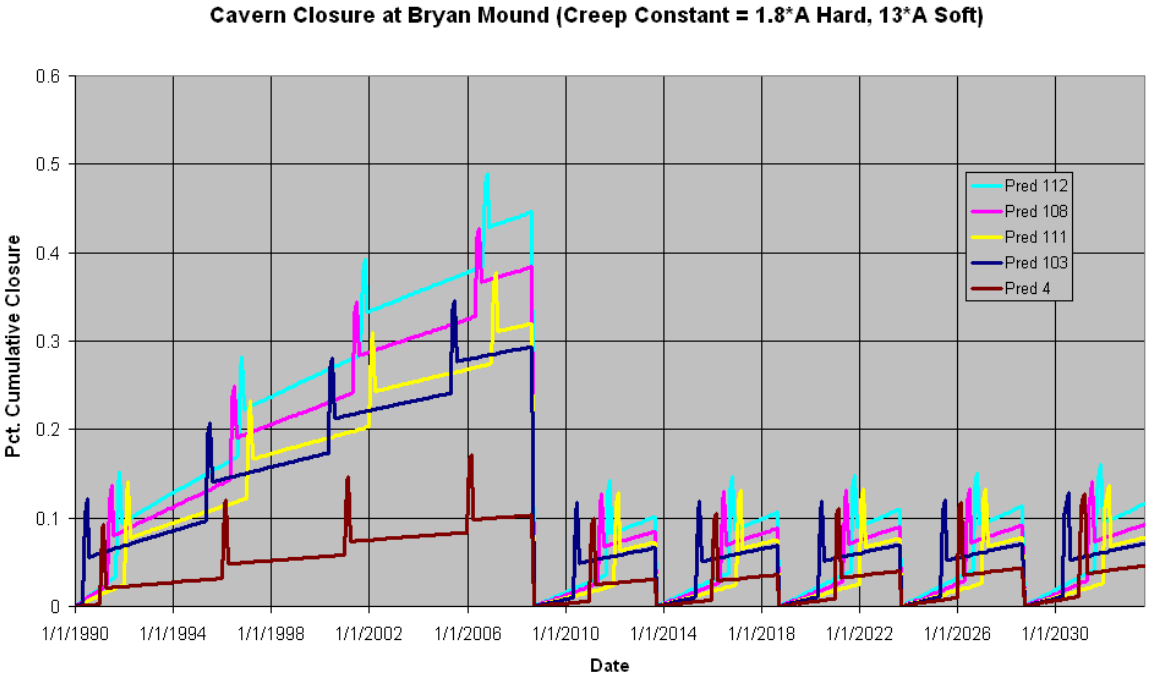

Figure 32. Predicted percentage closure of selected caverns in the Bryan Mound hard salt (corresponding to the caverns in Figure 14).

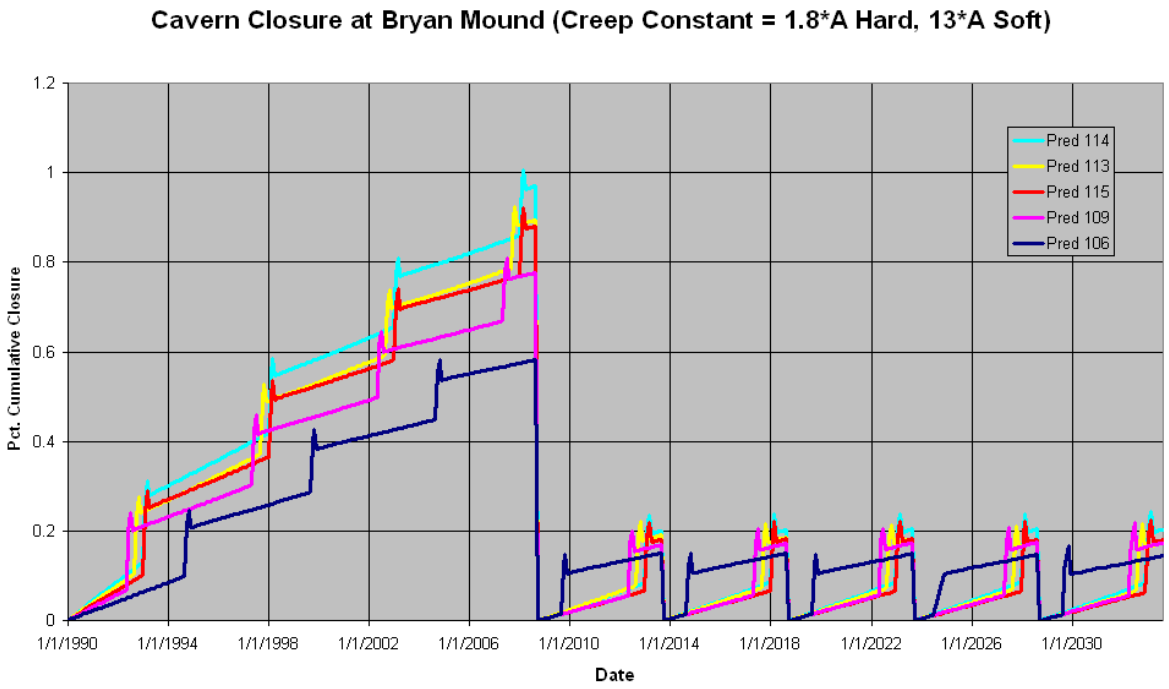

Figure 33. Predicted percentage closure of caverns in the Bryan mound soft salt (corresponding to the caverns in Figure 15).

4.3 AXIAL WELL STRAIN

The physical presence of wells and surface structures are not included in the finite element model, but the potential for ground deformation to damage these structures can be conservatively estimated by assuming that they will deform according to the predicted ground strains. At well locations, subsidence will primarily induce elongation of the axis of the well. Under these conditions, the cemented annulus of the wells may crack forming a horizontal tensile fracture that may extend around the wellbore. This may not result in vertical fluid migration along the casing, but could permit horizontal infiltration into ground waters. This may be a well vulnerability, especially in the caprock, where acidic ground waters may gain access to the steel casing and corrode it. More extensive damage could heavily fracture the cement which could result in a loss of well integrity in that leakage could occur from the cavern along the outside of the casing. Such leakage could result in flow to the surrounding environment, resulting in loss of product. The allowable axial strain for purposes of this report is assumed to be 0.2 millistrains in tension. This would be typical of cement with a compressive strength in the range from 2500 to 5000 psi (Thorton and Lew, 1983). It should also be noted that vertical well strain reduces the collapse resistance of the steel casings. For a typical SPR well located in the caprock, negligible resistance to casing collapse is predicted at 1.6 millistrains.

Figure 34 shows a history of the total vertical strain from the top of the salt dome (1040 feet depth) to the ceiling of the cavern for all the Bryan Mound caverns. The cement liner and steel casing thresholds are also shown on the plot. The segments of casing located within the salt vary in length between about 1900 and 2300 feet, with the exception being cavern 2 whose ceiling is

400 feet beneath the top of salt. All of the cavern wells in the soft salt section (highlighted with bold plot lines) are predicted to have exceeded the 0.2-millistrain threshold for the cement liners within a few years after their construction. This is similar to the results of the analysis of the West Hackberry salt dome, whose creep properties are nearly equal to the soft salt properties used here; nearly all the caverns experienced 0.2 millistrains of vertical strain within a few years of operation. The boreholes close to the center of the field exceed the 0.2-millistrain threshold through the 1990s and early-2000s, whereas the well strains for the outlying caverns in the hard salt remain below the threshold for many years after expansion begins. The 1.6-millistrain steel casing threshold is not predicted to be exceeded during the 25-year cavern expansion period. Because of these results, cement liner concerns exist for the soft salt caverns (106, 109, 113, 114,115); also, cavern 103 may experience similar problems, as it appears to reside in higher-creeping salt as well, based on the cavern closure information in Table 4.

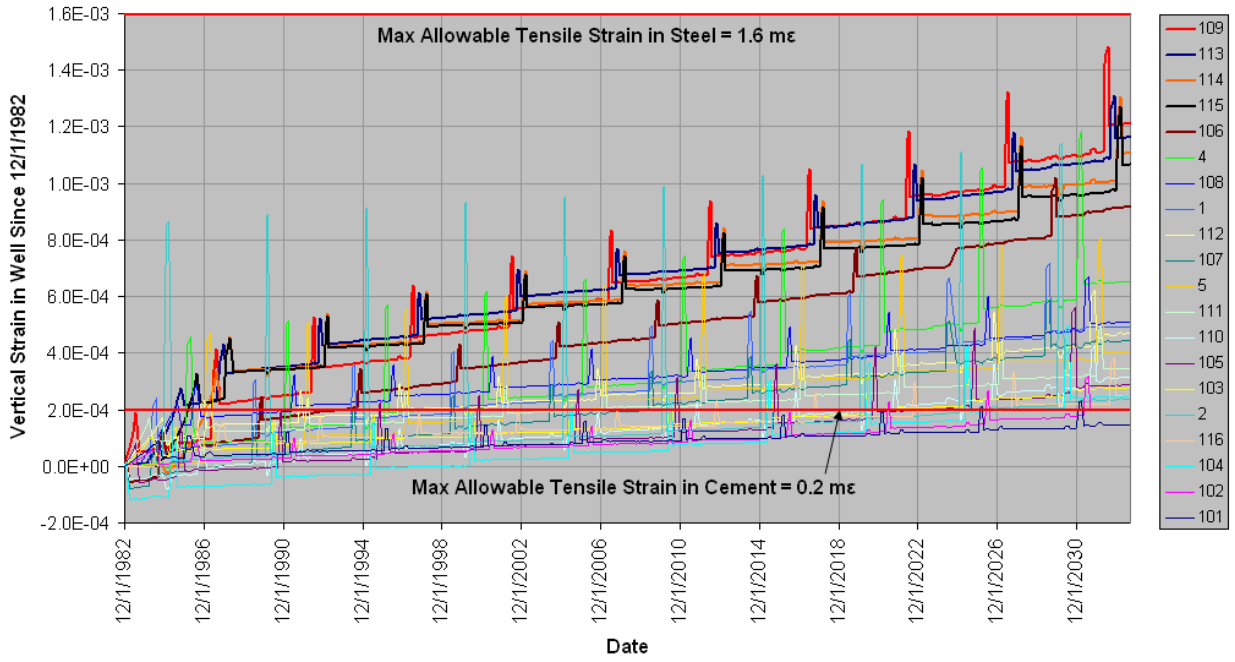

Figure 34. Total vertical strain, top of salt to cavern ceiling, for all Bryan Mound caverns.

The numbers presented in Figure 34 represent the entire length of the wells in the salt dome; it is also instructive to look at the total well strain in the caprock and in the overburden. Figures 35 and 36 show the total vertical strain for all the wells since 1982, within the overburden (surface to 760 feet depth) and the caprock (760 to 1040 feet depth, 280 feet total length) respectively. The strains here are calculated for shorter segments of well casing, so much higher strains would be expected. Figure 35 in particular presents a more severe prediction of the potential for well casing damage over some of the caverns. Wells for caverns 1, 107, 100 and 4 are near the steel casing strain threshold in the overburden in the year 2008, and other nearby wells may reach that threshold in 2010. Well casing concerns can also be expected as the caverns are enlarged. On the other hand, well strains within the shorter caprock region do not exceed the strain thresholds for cement or steel. However, the effect of the large strains in the overburden and salt sections of the well may manifest themselves anywhere along the length of the well. These calculations

would indicate that the potential for cement liner and steel casing failure in the cavern wells in the overburden is significant, and cement bond and casing inspection logs should be performed as part of operations and potential mitigating measures should be considered especially as the caverns are leached. The vertical strain predictions presented here should be correlated with known well casing problems to determine field-appropriate strain threshold values. Events that would indicate a possible casing/liner failure include loss of pressure during cavern integrity testing, measurable loss of oil during normal operating procedures, obstruction of borehole due to displacement of fractured casing and liner material. Also, fiber optic cameras and other types of logs sent down the boreholes might identify failure or corrosion areas. To date, there have been no indications that a steel casing or cement liner has failed in any Bryan Mound cavern, but the wells are not being logged. It is also possible that casing failures or yielding has occurred, but have yet to be detected. Because of the high strain values predicted for the current borehole liners, it is important to ascertain the current status of the liners and determine field-appropriate strain threshold values and possible mitigation procedures (Sattler, 2004).

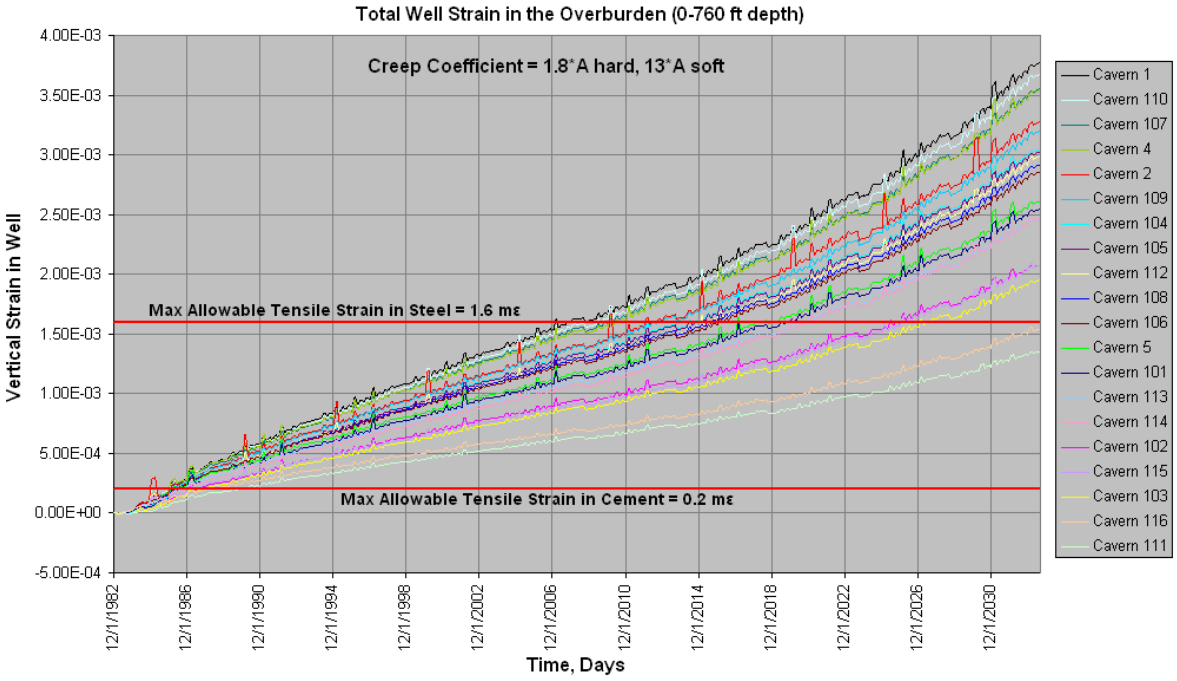

Figure 35. Total vertical strain within the overburden for all Bryan Mound caverns.

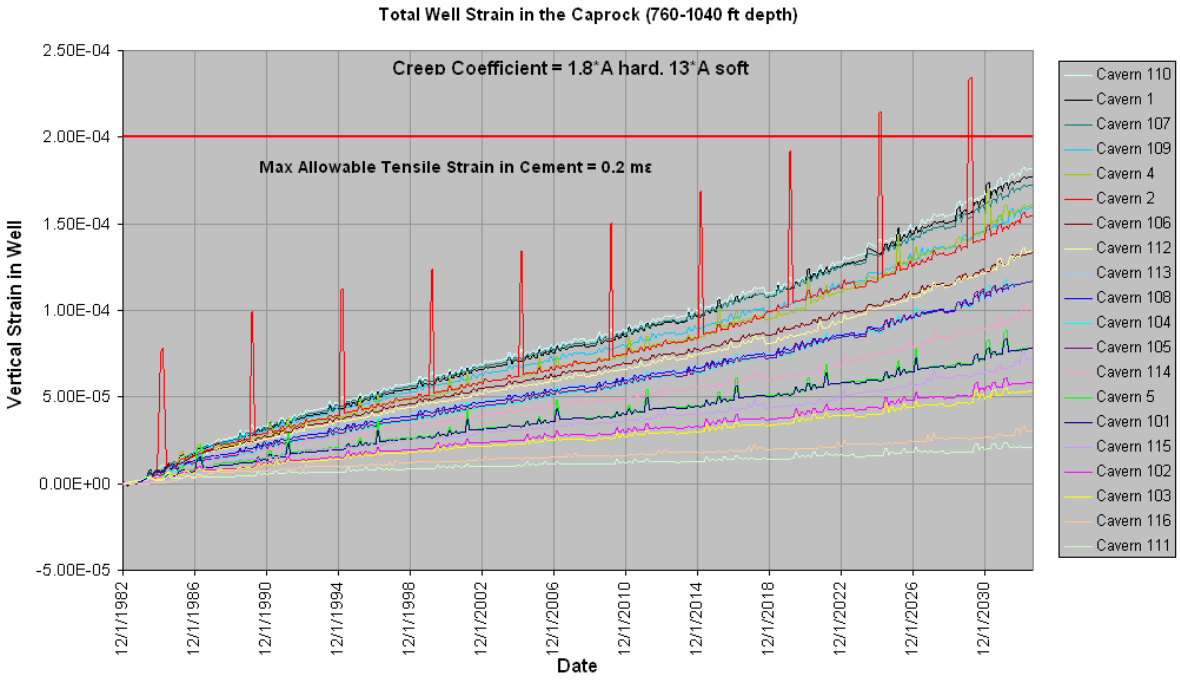

Figure 36. Total vertical strain within the caprock for all Bryan Mound caverns.

4.4 SURFACE SUBSIDENCE

The issue of surface subsidence is an important design and operations factor for surface facilities, especially for those located in flood prone areas, but subsidence also results in horizontal ground strains that can damage buildings, pipelines, and other infrastrusture. The SPR is currently over 25 years old and the life of the SPR may extent well into this century depending upon a number of factors, including oil consumption, import dependency, and geopolitical instability. Expected subsidence during a 100-year life of an SPR site on the order of up to ten feet is possible. Therefore, a reliable prediction of surface subsidence can be very valuable for site management. The plots in Figures 15, 16 and 17 that compared surface subsidences measured since 3/1/1985 to predicted values showed reasonable agreement using the Case #4 salt creep properties, but better agreement with the Case #3 properties. Figure 37 shows the predicted surface displacement with the assumed workover and cavern expansion cycles out to the year 2033 (when the facility is approximately 50 years old). The predictions indicate surface subsidence of an additional 0.75 feet between 2008 and 2033, to a total of 1.25 feet since 1985. The highest subsidence occurs over the caverns in the middle of the caverns field – caverns 1, 110, 107, and 4. Because the Case #4 properties underpredicted measurement subsidence by 25%-40%, the numbers in Figure 37 were adjusted based on a comparison between predictions from Case #3 and Case #4. The adjusted predictions are shown in Figure 38; here the predictions indicate an increase between 2008 and 2033 of 1.15 feet, to a total subsidence of 1.9 feet since 1985. By either prediction, the amount of expected subsidence is significantly smaller than that for other SPR sites.

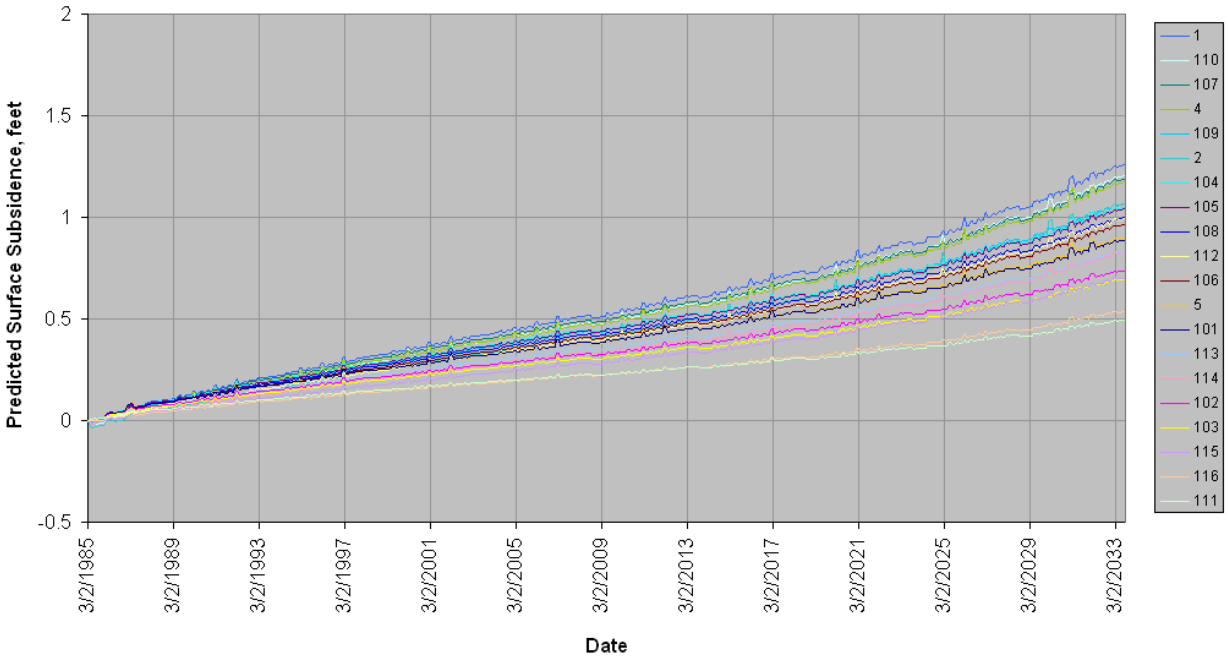

Figure 37. Predicted Bryan Mound Surface Subsidence History Using Case #4 Properties, to the year 2033.

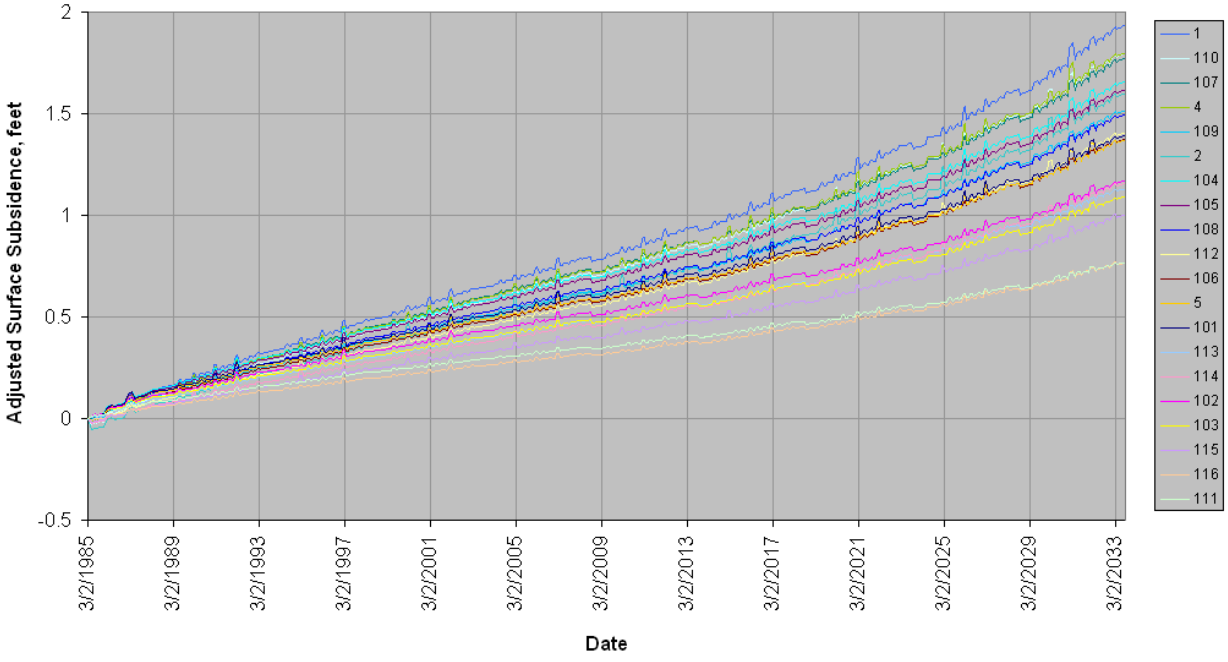

Figure 38. Adjusted Bryan Mound Surface Subsidence History Using Case #3 Properties, to the year 2033.

Structural damage on the surface is typically caused by large accumulated surface strains caused by surface subsidence. These strains can cause distortion, damage, and failure of buildings, pipelines, roads, bridges, and other infrastructure. Surface strains will accumulate in structures

over time, which increases the possibility of damage in older facilities. Typically, subsidence strains tend to be compressive in the central portion of the subsided area and become tensile in nature for areas farther removed. Some guidance and solutions are available to evaluate the predicted surface strains. These criteria vary from country to country, possibly due to different building codes and structural materials. Some examples of allowable strains are presented by Peng (1985). The criteria vary in some countries depending on application. For purposes of this paper, the allowable strain is taken to be 1 millistrain for both compression and tension. Criteria for shear strains have not been found, perhaps because they are less important. In practice, allowable strain limits for a structure are design specific and should be examined on a case-by-case basis.

The horizontal surface strains are related to the subsidence above the caverns. Typically, the region above the caverns undergo compressive horizontal stresses at the surface as the geologic units sag, but at some distance away from the cavern field the horizontal strains become tensile as the surface rises up to its original elevation. Figure 39 shows the maximum compressive and tensile strains at the surface as a function of time. This figure shows that neither 1-millistrain threshold for compressive or tensile strains will be exceeded by the year 2023. A better understanding of the effects of these strains can be gained by looking at contour plots of strain at the surface over the salt dome. Figure 40 shows the predicted minimum horizontal principal strains at the surface at four times: December 1982 (near beginning of SPR operations), August 2008 (approximately the current time), August 2014, and August 2033. By convention, negative strains are compressive, and positive are tensile. The minimum principal strains (i.e., maximum compressive strains) are centered above Cavern 1, and become steadily less compressive radially from that point. Tensile strains are not experienced until near the edge of the salt dome. Similarly, Figure 41 shows the predicted maximum horizontal strains at the surface. Several important observations can be made from these figures. First, the largest tensile strains, aligned primarily in the east-west direction, are generated on the surface above the edge of the dome. Second, the maximum principal strains in the center of the cavern field, above Cavern 1, do not exceed the compressive strain threshold, meaning the surface facilities and infrastructure in the vicinity of Cavern 1 are not expected to experience overly high compressive strains. The primary conclusion here is that, due to the expectedly small amount of surface subsidence, there should be no extraordinary concerns regarding strains imposed on surface facilities. Even if allowance is made for a higher expected subsidence as detailed in Figure 38, the horizontal surface strains are not expected to reach the 1-miilstrain threshold. Obviously, these results do not preclude standard facility monitoring and engineering procedures, but they do suggest that the issue of surface facility damage is not an urgent one.

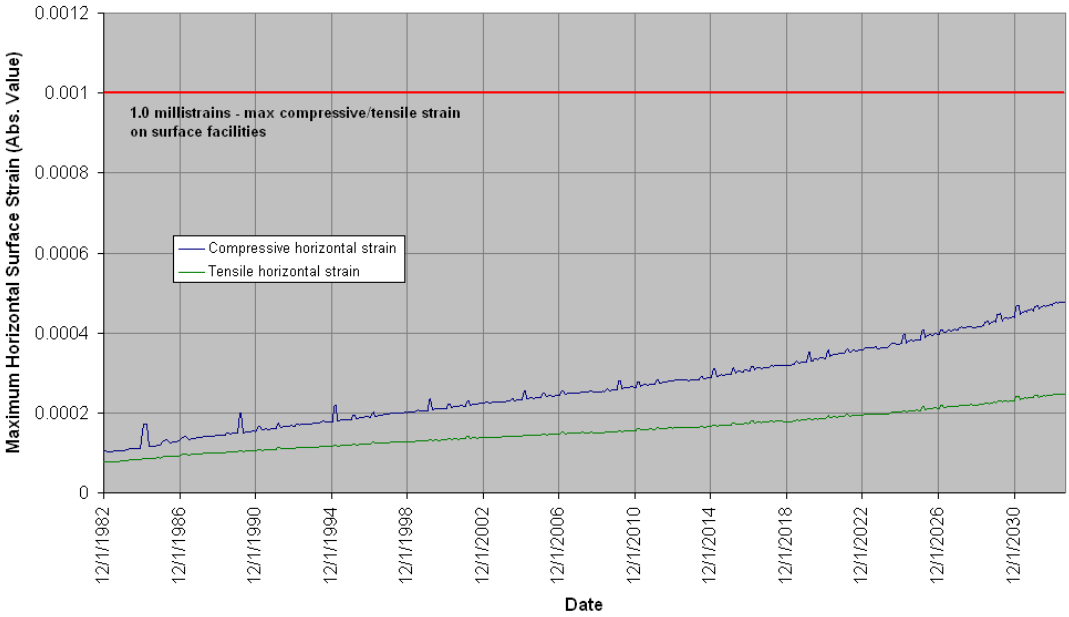

Figure 39. Maximum horizontal compressive and tensile strains as a function of time.

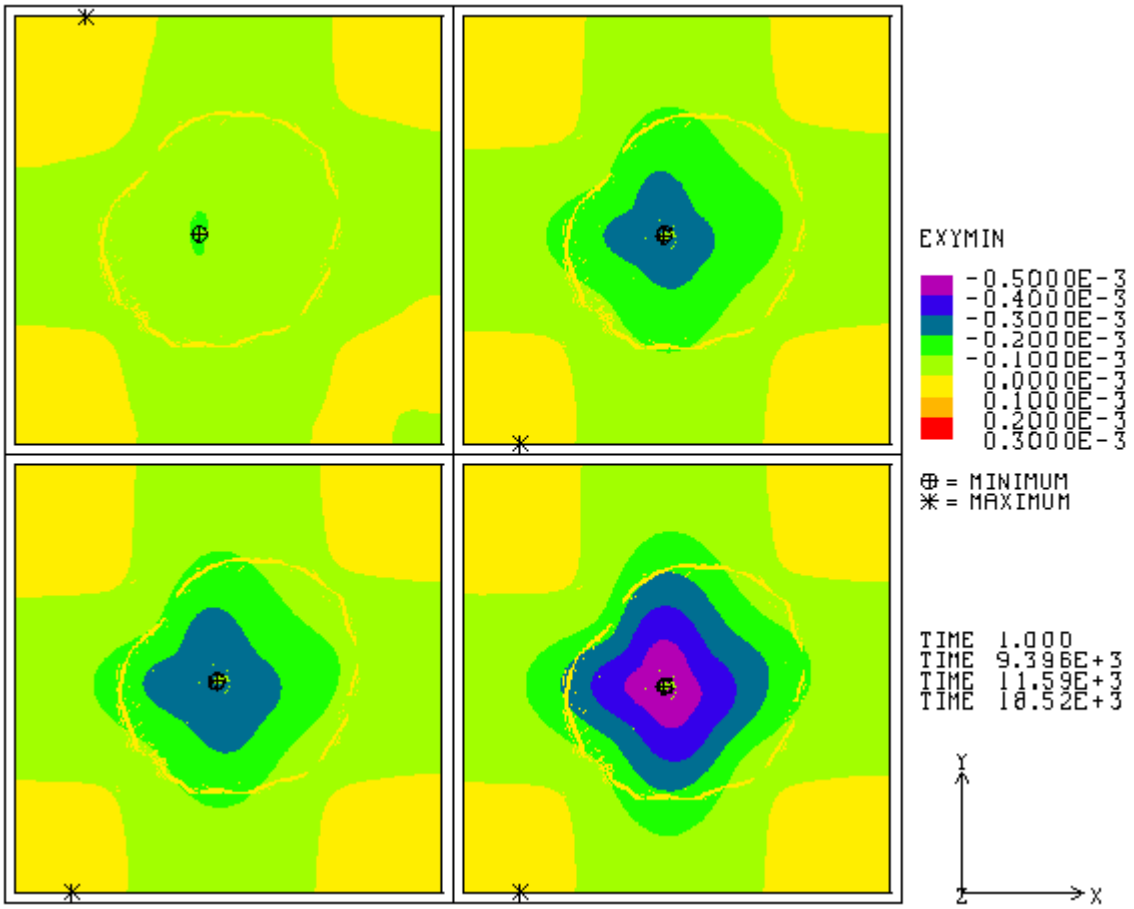

Figure 40. Minimum horizontal principal strains at the surface (negative strains in compression). (Time in days since 1982)

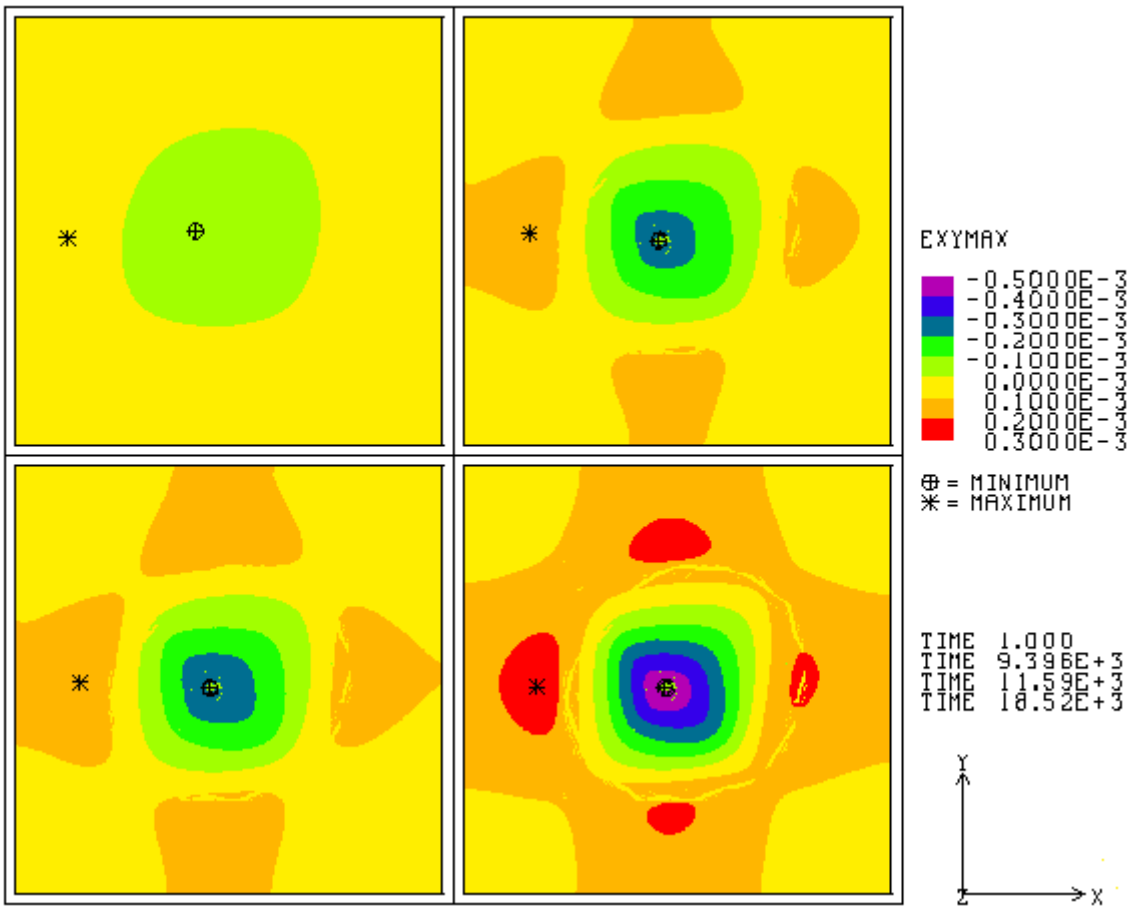

Figure 41. Maximum horizontal principal strains at the surface (positive strains in tension).

5. CONCLUSIONS

These analyses evaluated the twenty caverns at the Bryan Mound SPR site for their current condition and for potential enlargement. The analyses also examined the overall performance of the Bryan Mound site by evaluating surface subsidence, horizontal surface strains, and axial well strains. Finally, the analyses evaluated the possibility of nonlinear dilatancy behavior of the Bryan Mound salt, and its possible ramifications on cavern performance. The following conclusions were obtained from the results of the analyses:

- The Bryan Mound salt is, on average, a slow-creeping, or "hard" salt, as discussed in Munson (1998). However, upon examination of the cavern volume closure data, it is apparent that there is a wide variability in salt creep properties, and possibly other salt mechanical properties, throughout the dome. In particular, there appears the existence of a shear boundary running approximately southwest to northeast, and the caverns to the south of this boundary (106, 109, 113, 114, and 115) have much higher cavern closure rates, indicative of faster creeping salt. An exception to this is cavern 112, which also lies to the south of this potential shear boundary, but experiences much lower cavern closure than nearly all the caverns in the field. Even in the "hard" salt to the north of the boundary, there is a large variability in the correlation between measured and predicted cavern closure. Salt creep coefficients equal to 1.8 and 13 times the coefficient given by Munson (1998) for the hard and soft salts, respectively, were selected for this analysis, but they do not satisfactorily address the variability in cavern closure measured at the site.
- The times of highest potential of salt damage/salt falls are during large cavern pressure changes, such as depressurization or repressurization in workovers. Even at low cavern pressures, over time the stresses in the cavern walls will adjust to near isotropic conditions; there will be increased creep and cavern closure, but the potential for damage will dissipate as the cavern pressure remains constant.
- Caverns 1, 2, and 5 have some potential for experiencing dilatant or tensile damage to their surrounding salt during and after workovers. However, the potential regions for such damage are highly localized, dependent upon local cavern geometry, and are not expected to produce large-scale cracking of the salt. Cavern 5 has the greatest potential for operational problems due to dilatant damage, as the most likely damage zone is in the bottom of its upper lobe and in the neck extending to the lower lobe. This location makes the possibility for damage to the hanging string significant. There is no indication that enlarging caverns 1 and 2 (or leachings due to oil drawdowns) would have an adverse effect on cavern stability. Cavern 5 was not enlarged in this study, due to its difficult shape, but a targeted enlargement in the neck region should help out with stability and hanging string issues.
- The other caverns (101-116, and 4) have no significant issues regarding dilatant damage in the surrounding salt, and may be enlarged with no adverse effect on cavern stability.
- The predictions indicate surface subsidence of an additional 1.15 feet between 2008 and 2033, to a total of 1.9 feet since 1985. Subsidence-induced horizontal strains, which could impact surface facilities, are expected to remain under the 1-millistrain threshold for damage. Therefore, no subsidence-based structural issues have been identified for Bryan Mound.
- Vertical strains in the locations of the wells into the Bryan Mound caverns in some cases have already exceeded established thresholds for cement failure (0.2 millistrains) and steel casing collapse (1.6 millistrains). Of particular concern are the steel casings in the

overburden for the caverns near the center of the cavern field (such as 1, 107, 110, and 4), and the cement liners in the salt over the caverns in the soft salt (106, 109, 113, 114, and 115). The vertical strain predictions presented here should be correlated with known well casing problems to determine field-appropriate strain threshold values.

- Additional series of laboratory tests of salt from the Bryan Mound site would be beneficial, in light of the observed variabilty of the in situ properties. The original salt properties from Munson (1998) were developed from samples taken mainly from wells 107 and 108. It would be beneficial if additional tests were performed on samples from the soft salt south of the shear boundary (particularly 113, 114, and 115), from well 112, and from some of the other wells in the hard salt section. In addition, a combination of triaxial compression and triaxial extension tests, where the salt samples are tested to dilatant failure, would greatly enhance the existing knowledge of the failure envelope of the salt at the site.
- Log data, hanging string failure events, and sonar measurements can be used to monitor the status of the cavern at several points in time. However, these data points are sparse, so it is difficult to detect salt fall events unless an obvious failure (i.e., hanging string) occurs. Particularly because the caverns are between 20 and 60 years old, additional monitoring of the conditions of the cavern walls and well casings would be beneficial, particularly cement bond and casing inspections logs.

6. REFERENCES

- Ballard, S., and B. L. Ehgartner, 2000. *CaveMan Version 3.0: A Software System for SPR Cavern Pressure Analysis*, SAND2000-1751, Sandia National Laboratories, Albuquerque, New Mexico.
- Bauer, S. J., 1999. *Analysis of Subsidence Data for the Bryan Mound Site, Texas*, SAND99-1739, Sandia National Laboratories, Albuquerque, New Mexico.
- Blanford, M.L., M.W. Heinstein, and S.W. Key, 2001. *JAS3D. A Multi-Strategy Iterative Code for Solid Mechanics Analysis.* ***User's Instructions****, Release 2.0*. SEACAS Library, JAS3D Manuals, Computational Solid Mechanics / Structural Dynamics, Sandia National Laboratories, Albuquerque, New Mexico.
- DOE (U.S. Department of Energy), 2001. Design Criteria- Level III. US Department of Energy, Strategic Petroleum Reserve, New Orleans, Louisiana, November, 2001.
- Ehgartner, B.L. and S.R. Sobolik, 2002. *3-D Cavern Enlargement Analyses*, SAND2002-0526, Sandia National Laboratories, Albuquerque, New Mexico.
- Hogan, R. G., ed., 1980. *Strategic Petroleum Reserve (SPR) Geological Site Characterization Report: Bryan Mound Salt Dome*, SAND80-7111. Sandia National Laboratories, Albuquerque, NM.
- Lama, R.D. and V.S. Vutukuri, 1978. *Handbook on Mechanical Properties of Rocks – Testing Techniques and Results*, Series on Rock and Soil Mechanics, Vol. 3, No.2, Trans Tech Publications.
- Morgan, H.S. and R.D. Krieg, 1990. *Investigation of an Empirical Creep Law for Rock Salt that Uses Reduced Elastic Moduli*, SAND89-2322C, presented at the 31st U.S. Symposium on Rock Mechanics held in the Colorado School of Mines in June 18-20, 1990, Sandia National Laboratories, Albuquerque, New Mexico.
- Munson, D.E., 1998. *Analysis of Multistage and Other Creep Data for Domal Salts*, SAND98-2276, Sandia National Laboratories, Albuquerque, New Mexico.
- Neal, J.T., T.R. Magorian, and S. Ahmad, 1994. *Strategic Petroleum Reserve (SPR) Additional Geologic Site Characterization Studies Bryan Mound Salt Dome, Texas*, SAND94-2331. Sandia National Laboratories, Albuquerque, New Mexico.
- Peng, S.S., 1985. Coal Mine Ground Control. 2nd Ed., John Wiley and Sons, New York, New York.
- Preece, D.S. and J.T. Foley, 1984. *Long-Term Performance Predictions for Strategic Petroleum Reserve (SPR) Caverns*, SAND83-2343, Sandia National Laboratories, Albuquerque, New Mexico.
- Rautman, C.A. and A. Snider Lord, 2007. *Sonar Atlas of Caverns Comprising the U.S. Strategic Petroleum Reserve Volume 3: Bryan Mound Site, Texas*, SAND2007-6067, Sandia National Laboratories, Albuquerque, New Mexico.
- Sattler, A.R. Milestone Requirement: Subtask 1.1.4, activity a2--Prepare plan for running casing inspection and cement bond logs. Letter report to Robert E. Myers, December 6, 2004.

- Sobolik, S.R. and B.L. Ehgartner, 2007. *Analysis of Cavern Stability at the West Hackberry SPR Site,* Draft SAND report (final version to be released in 2009), Sandia National Laboratories, Albuquerque, New Mexico.
- Stein, J.S. and Rautman, C.A., 2005. *Conversion of the Bryan Mound Geological Site Characterization Reports to a Three-Dimensional Model*, SAND2005-2009, Sandia National Laboratories, Albuquerque, New Mexico.
- Thorton, C.H and I.P. Lew, 1983. *Concrete and Design Construction. Standard Handbook for Civil Engineers*, Chapter 8, 3rd ed., F.S. Merritt, editor, McGraw-Hill, New York, NY.
- Van Sambeek, L.L., J.L. Ratigan, and F.D. Hansen, 1993. *Dilatancy of Rock Salt in Laboratory Tests*, Int. J. Rock Mech. Min. Sci. & Geomech. Abstr. Vol. 30, No. 7, pp 735-738.
- Wawersik, W.R. and D.H. Zeuch, 1984. *Creep and Creep Modeling of Three Domal Salts – A Comprehensive Update*, SAND84-0568, Sandia National Laboratories, Albuquerque, New Mexico.

DISTRIBUTION:

U.S. Department of Energy (electronic copy only)
Strategic Petroleum Reserve Project Management Office
900 Commerce Road East
New Orleans, LA 70123
Attn: W. Elias at Elias. Wayne@SPR.DOE.GOV
R. Myers at Robert.Myers@SPR.DOE.GOV

U.S. Department of Energy (3)
Strategic Petroleum Reserve Program Office
1000 Independence Avenue, SW
Washington, D.C. 20585
Attn: D. Johnson, FE-421

1	MS	0706	D.J. Borns, 6312
5	MS	0706	B.L. Ehgartner, 6312
1	MS	0706	A.R. Sattler, 6312
1	MS	0706	D.E. Munson, 6312
1	MS	0706	C.A. Rautman, 6312
1	MS	0751	T.W. Pfeifle, 6315
5	MS	0751	S. R. Sobolik, 6315
1	MS	1002	S. Roehrig, 6300
1	MS	1395	B. Y. Park, 6821
1	MS	0701	J. A. Merson, 6310
1	MS	0376	J. G. Arguello, 1526
1	MS	0376	C. M. Stone, 1527
1	MS	0899	Technical Library, 9536 (electronic copy)

Electronic copy only to Wayne Elias at for distribution to DOE and DM


Sandia National Laboratories